

WHAT DOES CLUSTERING TELL US ABOUT THE BUILDUP OF THE RED SEQUENCE?

JEREMY L. TINKER¹ AND ANDREW R. WETZEL²

¹Berkeley Center for Cosmological Physics, University of California-Berkeley

²Department of Astronomy, University of California-Berkeley

Draft version October 25, 2018

ABSTRACT

We analyze the clustering of red and blue galaxies from four samples spanning a redshift range of $0.4 < z < 2.0$ to test the various scenarios by which galaxies evolve onto the red sequence. The data are taken from the UKIDSS Ultra Deep Survey, DEEP2, and COMBO-17. The use of clustering allows us to determine what fraction of the red sequence is made up of central galaxies and satellite galaxies. At all redshifts, including $z = 0$, the data are consistent with $\sim 60\%$ of satellite galaxies being red or quenched, implying that $\sim 1/3$ of the red sequence is comprised of satellite galaxies. More than three-fourths of red satellite galaxies were moved to the red sequence after they were accreted onto a larger halo. The constant fraction of satellite galaxies that are red yields a quenching time for satellite galaxies that depends on redshift in the same way as halo dynamical times; $t_Q \sim (1+z)^{-1.5}$. In three of the four samples, the data favor a model in which red central galaxies are a random sample of all central galaxies; there is no preferred halo mass scale at which galaxies make the transition from star-forming to red and dead. The large errors on the fourth sample inhibit any conclusions. Theoretical models in which star formation is quenched above a critical halo mass are excluded by these data. A scenario in which mergers create red central galaxies imparts a weaker correlation between halo mass and central galaxy color, but even the merger scenario creates tension with red galaxy clustering at redshifts above 0.5. These results suggest that the mechanism by which central galaxies become red evolves from $z = 0.5$ to $z = 0$.

Subject headings: cosmology: observations—galaxies:clustering

1. INTRODUCTION

In the redshift-zero universe we observe a distinct bimodality in the distribution of galaxies; the two populations are comprised of blue star-forming objects and red passively evolving objects (Strateva et al. 2001; Blanton et al. 2003a; Kauffmann et al. 2003b; Madgwick et al. 2003). Bimodality is clearly seen at $z \sim 1$ (Bell et al. 2004; Cooper et al. 2006; Willmer et al. 2006). Recent results detect this bimodality out to $z = 2$ and suggest that the red sequence exists at even higher redshifts (Kriek et al. 2008; Williams et al. 2009, hereafter W09). How this bimodality was created and has evolved is an outstanding problem in galaxy evolution and the history of star formation in the universe. In this paper we use the clustering of several bimodal galaxy samples spanning $0.4 < z < 2.0$ to test the various physical processes that may halt star formation within a galaxy and initiate its transition onto the red sequence.

There are three dominant physical mechanisms by which galaxies can migrate from the blue cloud to the red sequence: (1) Major mergers can rapidly exhaust the available gas within two galaxies in a burst of star formation, resulting in a passively evolving elliptical galaxy (e.g., Toomre & Toomre 1972; Negroponte & White 1983; Mihos & Hernquist 1996; Springel 2000); this idea has been developed in a more statistical fashion by Hopkins et al. (2008b,a). Since the galaxy merger rate is expected to increase with mass, this scenario implies a larger red fraction at higher halo mass. (2) Galaxies can be accreted onto a group-sized or cluster-sized dark matter halo; in this scenario, the new satellite halo (which we will refer to as a subhalo) is no longer able to accrete gas, and the gas already contained within the subhalo is subjected to both tidal forces and ram-pressure stripping. Thus star formation is predicted to be attenuated in satellite galaxies (e.g., Gunn & Gott 1972; Abadi et al. 1999; Wang et al. 2007; van den Bosch et al. 2008; Kimm et al. 2009). This

effect is observed in the color distributions of clusters of galaxies (e.g., Butcher & Oemler 1978, 1984; Hansen et al. 2009). (3) There is a halo mass scale above which star formation is significantly attenuated, either by virial shocks and related processes (Birnboim & Dekel 2003; Kereš et al. 2005, 2008; Dekel & Birnboim 2006; Cattaneo et al. 2006; Dekel & Birnboim 2008) or through feedback by active galactic nuclei, which is strongly correlated with halo mass (Croton et al. 2006; Bower et al. 2006; De Lucia & Blaizot 2007; Somerville et al. 2008). Many of these studies give rise to a critical mass scale of $\sim 10^{12} h^{-1} M_{\odot}$, above which shock heating within a halo is efficient and gas accretion enters the “hot mode” phase. Outstanding questions remain: When do these processes begin and how long do they persist? Which dominate at high redshift? How is the red sequence built over time?

In this paper, we analyze previously published clustering measurements of red (quiescent) and blue (star-forming) galaxies for three different surveys at three distinct redshifts. W09 presented clustering results from galaxies in the UKIDSS Ultra Deep Survey (UDS). At $1 < z < 2$, they demonstrate a clear bimodal sequence in the galaxy population between star-forming and quiescent galaxies, with the quiescent systems being significantly more clustered. At $0.7 < z < 1.2$, Coil et al. (2008) presented color-dependent clustering measurements from the Deep Extragalactic Evolution Probe (DEEP2) spectroscopic survey. Once again, the red galaxies showed stronger clustering at all scales than the blue galaxies for any magnitude threshold. Using the COMBO-17 photometric survey, Phleps et al. (2006) (hereafter P06) measured the clustering of blue and red galaxies at $0.4 < z < 0.8$, with similar results.

Our analysis of this clustering utilizes the halo occupation distribution (HOD; see, e.g., Peacock & Smith 2000; Seljak 2000; Scoccimarro et al. 2001; Cooray & Sheth 2002;

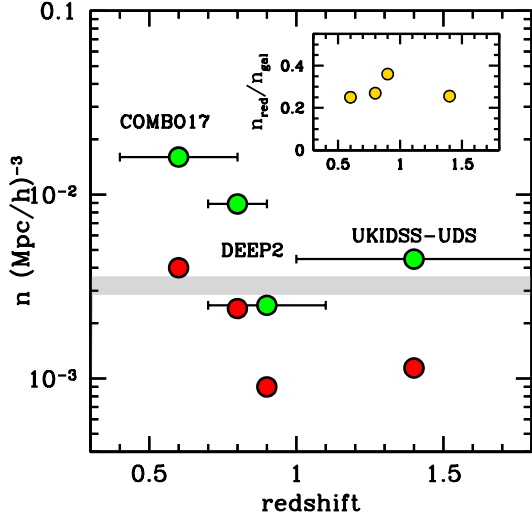


FIG. 1.— Green circles show the number densities of all (red+blue) galaxies in each sample as a function of their mean redshift. The horizontal error bars show the redshift range of each sample. The red circles show the number density of the red subsample in each survey. The inset panel shows the fraction of galaxies that are red in each sample, which, with the exception of the bright DEEP2 sample, is roughly 25%. The gray shaded band is the number density of galaxies brighter than L_* at $z = 0$ from the SDSS r -band luminosity function (Blanton et al. (2003b)).

Berlind & Weinberg 2002 for early works, and Zheng et al. 2007; van den Bosch et al. 2007; Tinker et al. 2009a for examples of more recent implementations of the framework). The HOD specifies the connection between galaxies and halos on a statistical basis, a connection that can be constrained through analysis of the two point correlation function $\xi(r)$.

Halo occupation analysis of bicolor clustering provides a test of many of the scenarios described above, since each one makes a distinct prediction for how red central galaxies occupy their halos and how they cluster. This enables us to address many questions related to the buildup of the red sequence. What fraction of the red sequence is created through satellite accretion? What is the quenching timescale for this process? At what halo mass scale—if any—do central galaxies transition from the blue cloud to the red sequence?

Unless otherwise stated, all calculations adopt a flat Λ CDM cosmology consistent with the latest constraints from CMB anisotropies (Dunkley et al. 2008). Our cosmological parameter set is $(\Omega_m, \sigma_8, h, n_s, \Omega_b) = (0.25, 0.8, 0.7, 0.95, 0.045)$. All distances are in comoving units, and all quoted magnitudes assume $h = 1$. Throughout this paper, we will use the terms “red” and “blue” interchangeably with “quiescent/passive” and “star forming.”

2. DATA AND ERRORS

2.1. Clustering in the UDS

The highest redshift clustering data comes from W09, in which the angular clustering, $w(\theta)$, of star-forming and quiescent galaxies were measured. The galaxies in the UDS are selected from observed-frame K -band photometry, complete down to $K < 22.4$. The sample analyzed here is a photometric redshift cut at $1 < z < 2$, with a median redshift of $z = 1.4$. W09 determined the rest-frame UVJ colors of the galaxies in a UDS fields. Within this color-color diagram, two distinct populations are seen out to $z = 2$, with one population having

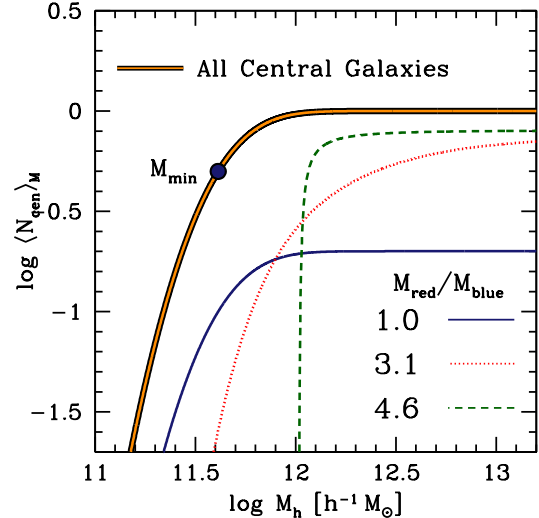


FIG. 2.— Examples of various central occupation functions for full samples and red galaxy subsamples. The thick curve shows a typical $\langle N_{\text{cen}} \rangle_M$ for central galaxies that matches the UDS sample. The three thin curves show various f_{Rcen} models that all have the number of red central galaxies, 20% of the number of all central galaxies. The solid curve is a model in which $f_{\text{Rcen}} = 0.2$ at all masses, yielding $M_{\text{red}}/M_{\text{blue}} = 1$. The dotted curve shows a model with a broad, smooth transition from halos hosting entirely blue central galaxies at low masses to predominantly red central galaxies at the group and cluster scale, yielding $M_{\text{red}}/M_{\text{blue}} = 3.1$. This model is similar to a scenario in which central galaxies become red through major mergers. The dashed curve shows a model that contains a critical mass scale at $M = 10^{12} h^{-1} M_{\odot}$, above which 80% of central galaxies are red, yielding $M_{\text{red}}/M_{\text{blue}} = 4.6$. This model is similar to a scenario as outlined by Dekel & Birnboim (2006).

star formation rates on average an order of magnitude higher than the other. W09 found that the clustering amplitude of red galaxies is nearly a factor of two higher than that of blue galaxies at large scales.”

The errors presented in W09 are bootstrap errors only, accounting for shot noise but without any estimation of sample variance. To place more robust errors on these data we use a high-resolution N-body simulation performed by Martin White using his TPM code (White 2002). The simulation volume is $720 h^{-1} \text{Mpc}$ per side with 1500^3 particles, yielding a mass resolution of $7.67 \times 10^9 h^{-1} M_{\odot}$ per particle. The cosmology of the simulation is the same as that assumed throughout this paper. Using the best-fit HOD model (utilizing W09 errors only; see in §3 for details on HOD fitting), the halos in the simulation were populated with red and blue galaxies matching the best-fit occupation functions of each. Although the photometric redshift cut in the W08 sample is $1 < z < 2$, the redshift distribution, $N(z)$ falls off rapidly after $z = 1.6$, and the fraction of galaxies at $z > 1.7$ is small. The box length itself is not long enough to cover the comoving distance from $1 < z < 1.7$ (roughly $1 h^{-1} \text{Gpc}$). To circumvent this problem, we reflected the box around the x and y axes, creating a volume 4 times larger, then rotated the resulting shape about the z axis by an angle of 45° . Within this volume there is a cuboid with xyz dimensions $720/\sqrt{2} \times 720/\sqrt{2} \times 720$ that fully utilizes the original volume of the simulation with no double-counting of any structure within the box (here the y axis is the line of sight). The extra box length comes at the expense of the one other dimension, but the resulting volume has sufficient comoving depth to model the W09 data within $1 < z < 1.8$.

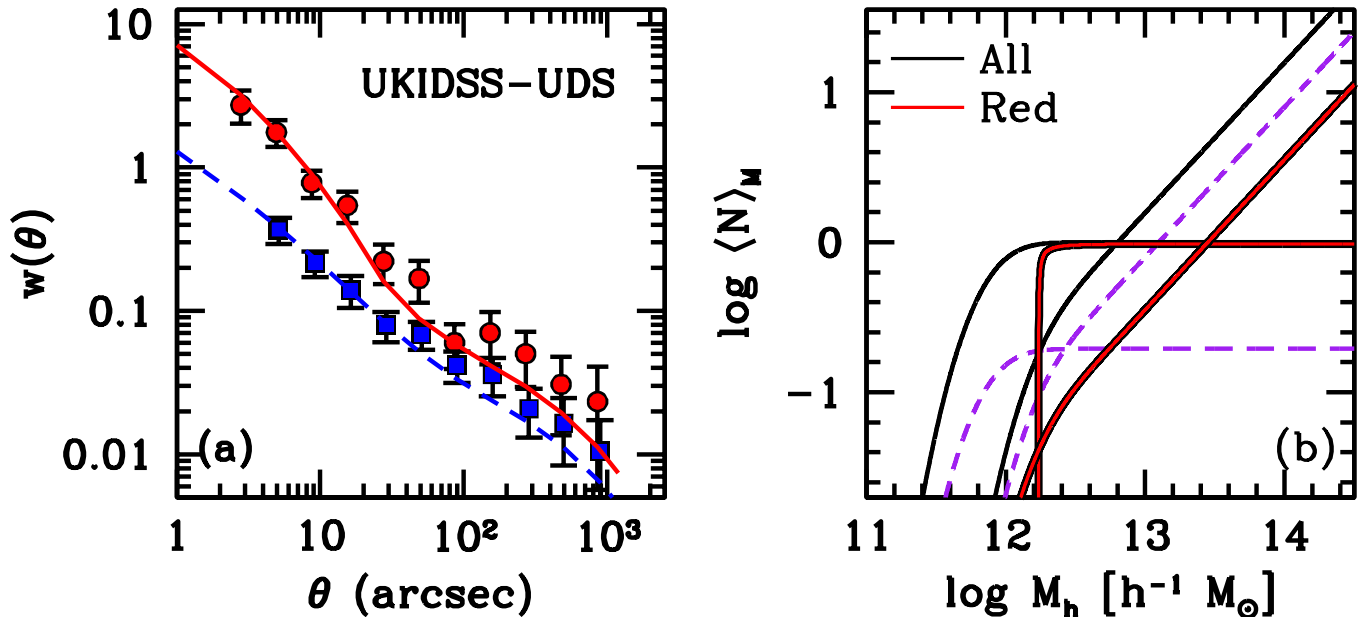


FIG. 3.— Panel (a): Clustering measurements from Williams et al. (2009) for quiescent and star-forming galaxies in the Ultra Deep Survey of UKIDSS within the redshift range $1 < z < 2$. Circles represent the quiescent subsample, while squares represent the star-forming galaxies. The solid and dotted curves show the best-fit HOD model for quiescent and star-forming galaxies, respectively. Panel (b): Halo occupation functions from the best-fit model. The thin solid curves indicate the HOD for *all* galaxies in the sample; the horizontal curve with a Gaussian cutoff at $M \lesssim 10^{11.8} h^{-1} M_\odot$ represents all central galaxies, while the power-law curve represents satellite galaxies. The thick, red curves indicate the fraction of these galaxies that are quiescent (red). The dashed curves represent a model in which $f_{\text{Rcen}} = 0.22$ independent of halo mass. This model is within the 2σ lower limit on the HOD from the clustering data.

Given the angular area of the the UDS, 0.7 deg^2 , 140 independent lines of sight could be obtained from the simulation. In each line of sight, we calculate $w(\theta)$ with the Landy & Szalay (1993) estimator, as in done in W09. Ideally, a full error analysis should include the entire covariance matrix of both the red and blue clustering measurements, which, since they are measured from the same patch of sky, will be correlated. The 140 realizations are not sufficient to obtain a reliable estimate of the covariance, so throughout this paper we use diagonal errors only on the W08 data. This renders the parameter constraints obtained somewhat suspect. To aide in the constraining power of these data, and to help make up for the lack of an estimate of the covariance between the red and blue galaxies, we also use the relative bias of red and blue clustering. This quantity is less effected by sample variance because the amplitudes of red and blue galaxies in a given patch of sky will move in concert if the overall clustering of that patch varies from the universal mean (Seljak et al. 2009). Taking the ratio of $w(\theta)$ at each of the four data points at $\theta > 100''$, where the data are firmly in the two-halo regime, the relative bias $b_{\text{red}}/b_{\text{blue}} = 1.42$. Using the same approach on $w(\theta)$ from the mocks, the variance of $b_{\text{red}}/b_{\text{blue}}$ is 11%. We also incorporate the error in the number density of each subsample, which we estimate from the variance of the mocks. These errors are 12% for the red galaxies and 14% for the blue galaxies.

Finally, to model $w(\theta)$, information on the redshift distribution, $N(z)$, is required. The photometric redshift distribution is close to a top-hat function from $1 < z < 1.8$, but due to uncertainties in the photometric redshifts, the true $N(z)$ is somewhat broader. An estimate of the underlying $N(z)$ using the errors in the photo- z 's, kindly provided by R. Williams, is used in all analytic calculations. The methodology for obtaining the

estimated $N(z)$ is described in W09 and Quadri et al. (2008).

2.2. Clustering Measurements from the DEEP2 Survey

Measurements of the clustering of blue and red galaxies at $z \sim 0.8$ in the DEEP2 survey have been published by Coil et al. (2008). Being a spectroscopic redshift survey, DEEP2 is superior to the UDS in that the true redshift-space correlation function can be estimated. This quantity, referred to as $\xi(r_p, \pi)$, where r_p is the projected separation of galaxy pairs and π is the line-of-sight separation, can be integrated along π to obtain a measurement of the projected galaxy correlation function, $w_p(r_p)$. The use of a projected quantity ameliorates the effect of redshift-space distortions on both large scales from coherent infall into overdense regions (e.g., Kaiser 1987; Fisher 1995; Hamilton 1998; Scoccimarro 2004) and small scales from non-linearities and virial motions of satellite galaxies (e.g., Davis & Peebles 1983). The quantity $w_p(r_p)$ is only free of redshift space effects if the projection is over a sufficiently large line-of-sight distance (formally, the projection of the real-space and redshift-space correlation functions are identical if the projection is extended to infinity). Due to the small sample size of DEEP2, 3 square degrees, the statistics are not good enough to estimate $\xi(r_p, \pi)$ out to large values of π , thus the Coil et al. (2008) measurements are integrated over the range $\pm 20 h^{-1} \text{ Mpc}$. This π_{max} is large enough to eliminate non-linear redshift-space effects, but large-scale infall will contribute to the measured amplitude of $w_p(r_p)$ at $r_p \gtrsim 5 h^{-1} \text{ Mpc}$.

Our goal in this paper is to probe the galaxy and halo mass scale at which the transition to the red sequence begins. Thus we focus on the DEEP2 results for the magnitude threshold sample of $M_B < -19.5$, the faintest sample published. For the blue galaxies, the median redshift is 0.81, while for the red

galaxies the median redshift is 0.77. In practice we use $z = 0.79$ as the redshift of the combined red-blue analytic model, noting that our results depend little on the assumed redshift in the range specified. As a consistency check on our results, we also consider a bright sample of galaxies with $M_B < -20.5$. The median redshifts for the blue and red subsamples are 0.99 and 0.88, respectively.

Coil et al. (2008) estimated errors from the sample-to-sample variance from 10 independent fields. Since the volume of this sample is $\sim (100h^{-1}\text{Mpc})^3$, sample variance is a concern. As with the UDS sample, we also include the uncertainties in the number densities for each sample. We estimate these uncertainties from mocks created from the sample N-body simulation as above, but now each mock is a cube with the same volume as the observational sample. The mocks are created from using the best-fit HOD parameters under the assumption of no errors in the number density. The uncertainties in the abundances are 11% and 13% for the blue and red subsamples, respectively.

All the samples in Coil et al. (2008) are separated into blue and red subsamples by a tilted cut in color-magnitude space, $(U - B) = -0.023(M_B + 21.62) + 1.035$. Using this cut, $\sim 27\%$ of the galaxies in the faint sample are red, while $\sim 36\%$ of the objects in the bright samples are classified as red. As opposed to the UVJ method of defining samples in the UDS, a single color cut can be subject to dust contamination. We will discuss the possible systematics of this effect in §6.

2.3. Clustering Measurements from COMBO-17

The COMBO-17 survey is a photometric survey covering 0.78 deg^2 with 17 broad- and medium-band filters, producing high-precision photometric redshifts (see Wolf et al. 2003, 2004 for details of the survey). Galaxies are identified in observed-frame R -band, from which P06 created a volume-limited sample of galaxies down to $M_B < -18$. The photometric redshifts are accurate enough to yield measurements of $\xi(r_p, \pi)$ and $w_p(r_p)$ at a redshift of $z = 0.6$, presented in P06. Unlike the DEEP2 sample, in which $w_p(r_p)$ is obtained from integrating $\xi(r_p, \pi)$ out to $20 h^{-1}\text{Mpc}$, P06 integrate out to $100 h^{-1}\text{Mpc}$ using the direct measurements, then continue out to $200 h^{-1}\text{Mpc}$ using a linear theory model set to match the amplitude of the data at $\pi = 100 h^{-1}\text{Mpc}$. With this approach, redshift-space distortions are eliminated in the estimate of $w_p(r_p)$, provided that the linear theory model is accurate. Error bars are estimated from jackknife sampling of the COMBO-17 survey. Although P06 present measurements of the covariance matrix of both the red and blue subsamples, the matrices themselves are too noisy to be properly inverted. We use the diagonal errors obtained from the jackknife method in our analysis, but it should be noted that the matrices presented in Phleps et al. (2006) show that $w_p(r_p)$ becomes correlated outside of $r_p \sim 1 h^{-1}\text{Mpc}$. We assume the same uncertainties in the number densities as for the faint DEEP2 sample.

Utilizing the wide wavelength coverage of the 17 photometric bands, Phleps et al. (2006) used spectral-energy distribution (SED) fitting to break their sample of galaxies into active and passive types. The template spectra used in the fitting comprise a two-dimensional age/reddening sequence to remove the effect of dust on the classification of galaxies. A $U - V$ color cut based on the prescription of Bell et al. (2004) is then used to divide the sample into red and blue galaxies. This cut is a function of M_V and redshift.

2.4. Comparison of Surveys

These three surveys make up a heterogeneous collection of samples that vary in the bands, magnitude limits, and definitions of red and blue. It is perhaps more productive to look at the number densities rather than the luminosities—the number density of a threshold sample of galaxies correlates strongly with the mean halo mass scale being probed. The halo mass function also evolves from $z = 1.4$ to $z = 0.6$; the abundance of massive halos increases dramatically, while the number of $M \lesssim 10^{11}$ halos evolves only weakly. At the redshift of the UDS, the nonlinear halo mass scales—where the bias is approximately unity—is $1.7 \times 10^{10} h^{-1} M_\odot$, while at $z = 0.6$ it is $3.1 \times 10^{11} h^{-1} M_\odot$. At all redshifts, the halo mass scale probed by each sample is above this nonlinear scale, implying that any difference in the halo masses probed by red and blue galaxies will produce differences in the large-scale clustering.

The mean redshifts, redshift ranges, and number densities of the galaxy samples are shown in Figure 1. Ignoring the bright DEEP2 sample for the moment, the number density in our samples increases by roughly a factor of 3 from $z \sim 1.4$ to $z \sim 0.6$. Thus COMBO-17 is probing the clustering of lower-mass halos than either DEEP2 or the UDS. However, the fraction of galaxies that are red or passive is roughly constant at $\sim 25\%$.

3. METHODS

3.1. The Halo Occupation Distribution for a Threshold Sample of Galaxies

Before describing our model for the occupation of galaxy samples defined by color, we start by defining the halo occupation of all galaxies, red and blue together. For galaxy samples that are complete down to a given luminosity threshold, halo occupation is broken into two distinct parts: galaxies that reside in the center of a dark matter halo and satellite galaxies that are within the virial radius of the halo but are distributed throughout the halo.

For central galaxies, we parameterize the central occupation function as

$$\langle N_{\text{cen}} \rangle_M = \frac{1}{2} \left[1 + \text{erf} \left(\frac{\log M - \log M_{\text{min}}}{\sigma_{\log M}} \right) \right]. \quad (1)$$

Equation (1) yields a smooth transition between halos that are too small to contain galaxies bright enough to be included in the given sample ($M \ll M_{\text{min}}$) and halos that are massive enough such that they will always contain a galaxy at their center bright enough to be included ($M \gg M_{\text{min}}$). Formally, M_{min} is defined as the halo mass at which a galaxy has a 50% probability of containing a central galaxy in the sample. The parameter $\sigma_{\log M}$ controls how rapid the transition is between zero and one central galaxies. Physically, $\sigma_{\log M}$ represents the scatter in halo mass at the luminosity threshold defined by the sample, under the assumption that this scatter takes the form of a lognormal distribution. Equation (1) is the mean number of central galaxies; because there can only be one or zero central galaxies in a halo, the scatter about that mean is defined by a nearest-integer distribution. Low-redshift estimates of the mass-luminosity scatter yield values between 0.2 and 0.6, depending on luminosity (Tinker et al. 2006, 2007; Zheng et al. 2007; van den Bosch et al. 2007; More et al. 2009). For the UDS and COMBO-17 samples we set $\sigma_{\log M} = 0.3$ while for both DEEP2 samples we set $\sigma_{\log M} = 0.6$. The motivation

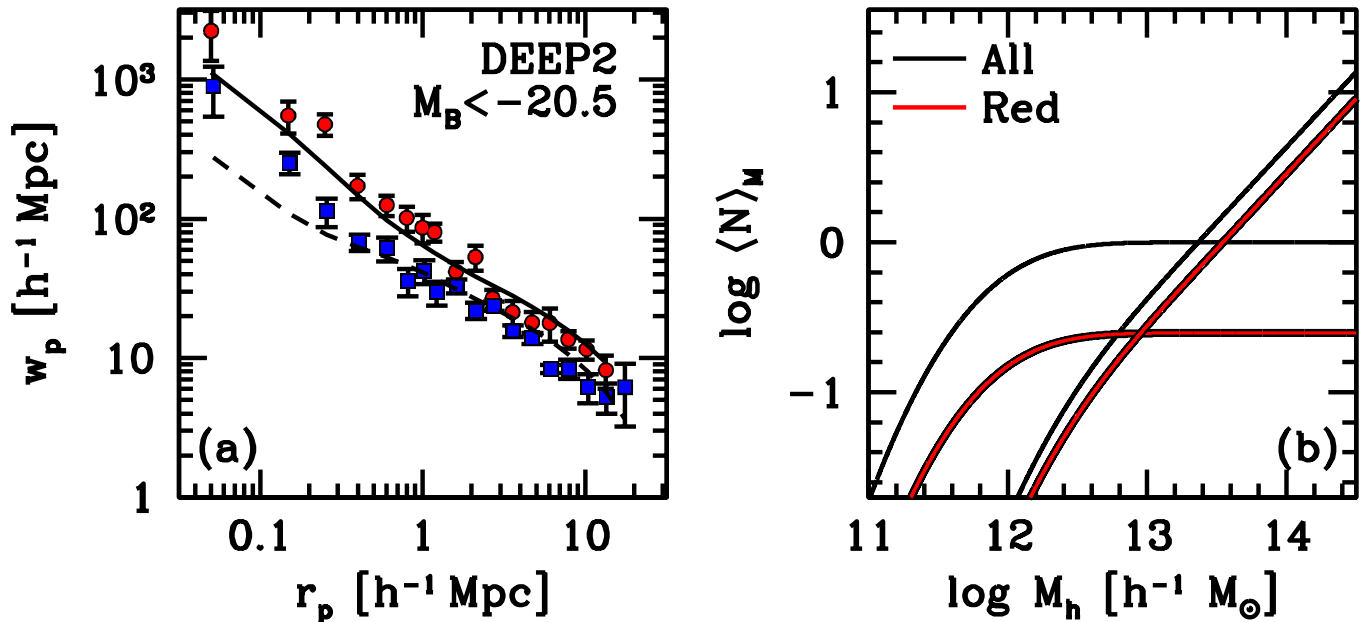


FIG. 4.— Panel(a): Measurements of the projected correlation function for galaxies with $M_B < -20.5$ in DEEP2 by Coil et al. (2008). The sample has a median redshift of $z \sim 0.9$. The circles and squares represent the measurements for red and blue galaxies, respectively. The solid and dashed curve represent the HOD model fits for red and blue galaxies, respectively. Panel (b): The best-fit occupation functions for all galaxies in the sample (thin solid curves) and red galaxies (thick curves). The model results imply that there is no threshold mass scale at which central galaxies preferentially become red; the higher clustering amplitude of red galaxies is produced by the high fraction of red satellite galaxies.

for the higher $\sigma_{\log M}$ for DEEP2 springs from the observed clustering amplitude of DEEP2 galaxies; the large-scale amplitude of $w_p(r_p)$ is somewhat lower than predictions using the WMAP5 cosmology and a reasonable bias model (see Wetzel & White 2009). This could imply larger magnitude errors or sample variance in the data. Allowing $\sigma_{\log M}$ to be a free parameter drives the best-fit values to physically unrealistic regions on parameter space. Fixing these values, rather than allowing them to be free parameters, does not bias our results.

For satellite galaxies, we parameterize the mean satellite occupation function as

$$\langle N_{\text{sat}} \rangle_M = \frac{1}{2} \left[1 + \operatorname{erf} \left(\frac{\log M - \log 2M_{\text{min}}}{\sigma_{\log M}} \right) \right] \left(\frac{M}{M_{\text{sat}}} \right)^{\alpha_{\text{sat}}}. \quad (2)$$

At halo masses well above the minimum mass scale, the number of satellite galaxies scales as a power-law with index α_{sat} and normalization M_{sat} . This is well-motivated from the results of hydrodynamical cosmological simulations (e.g., White et al. 2001; Berlind et al. 2003; Zheng et al. 2005) as well as high-resolution collisionless simulations (e.g., Kravtsov et al. 2004; Conroy et al. 2006; Wetzel & White 2009). In equation (2), the satellite occupation function has a cutoff of the same functional form as $\langle N_{\text{cen}} \rangle_M$, but with a transition mass a factor of two larger than that for central galaxies. This cutoff prevents halos with a low probability of containing a central galaxy from having a higher probability of containing a satellite galaxy in the sample, and is also motivated from the numerical results listed above. We assume that the scatter about the mean $\langle N_{\text{sat}} \rangle_M$ is Poisson (Kravtsov et al. 2004; Zheng et al. 2005).

We set $\alpha_{\text{sat}} = 1$ for all samples. There is strong theoretical and observational evidence for such a prior. High resolu-

tion dark matter simulations find that the subhalo mass function is nearly self-similar (Gao et al. 2004; De Lucia et al. 2004; Kravtsov et al. 2004), thus if satellite luminosity is tightly correlated with subhalo mass¹ the number of satellites above a given luminosity should scale linearly. Both cosmological hydrodynamic simulations and semi-analytic models of galaxy formation find that this scaling is not broken with the inclusion of baryonic physics (White et al. 2001; Zheng et al. 2005; Croton et al. 2006; Harker et al. 2007). Observationally, there is some discrepancy in the measured in clusters. Lin et al. (2004) find a value of $\alpha_{\text{sat}} < 1$, while Kochanek et al. (2003) find $\alpha_{\text{sat}} = 1.10 \pm 0.09$ (for a sample that contains significant overlap with the Lin et al. 2004 sample). Collister & Lahav (2005), using a much larger sample of galaxy groups from the 2PIGG catalog (Eke et al. 2004), find $\alpha_{\text{sat}} = 0.99$. Yang et al. (2008) find $\alpha_{\text{sat}} \approx 1$ from a group catalog constructed from the spectroscopic galaxy sample in DR4 of the SDSS. In the largest sample of galaxy clusters to date, the maxBCG cluster catalog (Koester et al. 2007), the results are also consistent with $\alpha_{\text{sat}} = 1$ (Hansen et al. 2009). We will discuss the effect of leaving α_{sat} as a free parameter for both red and blue samples in §6.

3.2. Separating Galaxies into Red and Blue

Many previous studies have presented halo occupation modeling of red and blue galaxy clustering (Scranton 2003; Magliocchetti & Porciani 2003; Zehavi et al. 2005; P06; Tinker et al. 2008b; Skibba & Sheth 2009). We will present a somewhat modified approach to color-dependent HOD modeling that is an extension of Tinker et al. (2009a).

¹ As noted in Nagai & Kravtsov (2005), Vale & Ostriker (2006), Conroy et al. (2006), Wang et al. (2006), and Wetzel & White (2009), satellite luminosity or mass correlates best with the mass (or circular velocity) of the subhalo at the time it is accreted, rather than the time it is observed.

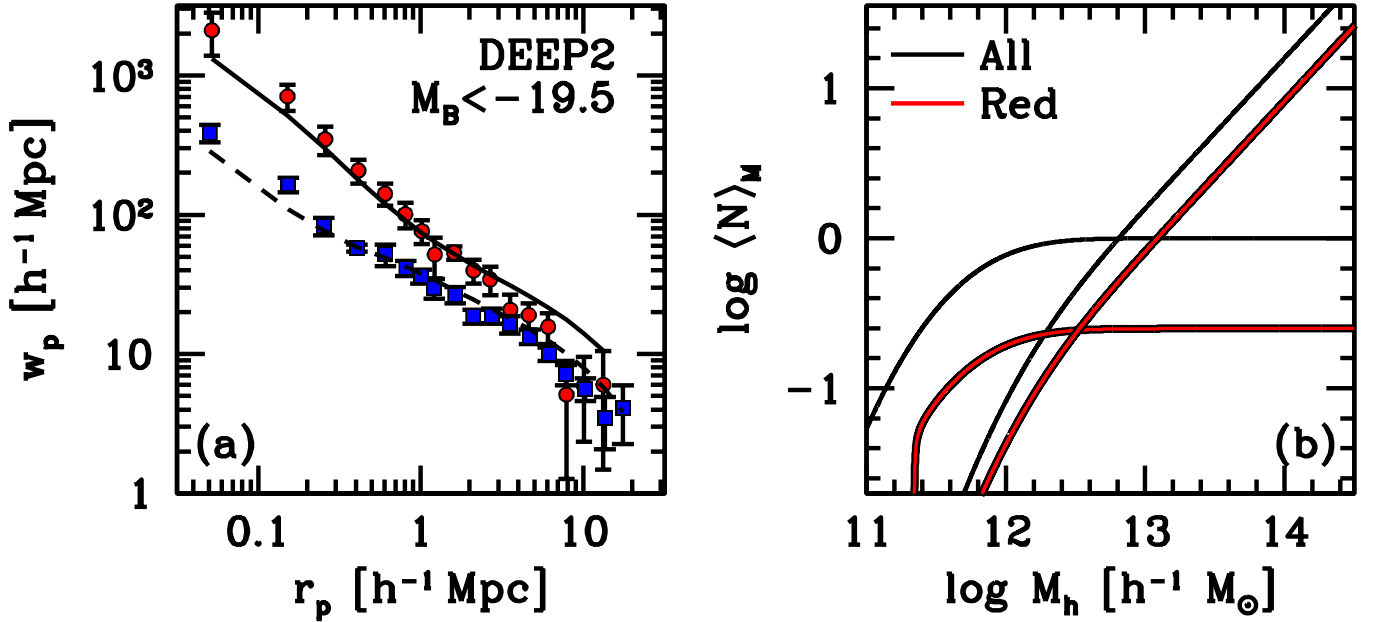


FIG. 5.— Panel (a): Measurements of the projected correlation function for galaxies with $M_B < -19.5$ in DEEP2 by Coil et al. (2008). The sample has a median redshift of $z \sim 0.8$. The circles and squares represent the measurements for red and blue galaxies, respectively. The solid and dashed curve represent the HOD model fits for red and blue galaxies, respectively. Panel (b): The best-fit occupation functions for all galaxies in the sample (thin solid curves) and red galaxies (thick curves). The asymptotic fraction of central galaxies that are red, f_{Rmax} , is set to be 0.25 to match the results from Figure 4. As with the bright sample from DEEP2, the HOD results for this sample imply that there is no preferred mass scale for red central galaxies; increased clustering of red galaxies is due mostly to f_{Rsat} , which is nearly twice as high as the overall fraction of red galaxies in this sample.

For satellite galaxies, we utilize a simple model to separate red and blue subsamples: a constant fraction of satellites, f_{Rsat} , are red, independent of halo mass. Previous models for low-redshift color-dependent data, ie Zehavi et al. (2005), allow this red satellite fraction to vary with halo mass. But in most samples investigated by Zehavi et al. (2005) and Tinker et al. (2008b), as well as our own tests, the best-fit models have little to no variation of f_{Rsat} with M . In the DEEP2 galaxy group catalog of Gerke et al. (2007), the red fraction is independent of group richness, supporting our assumption that the f_{Rsat} is independent of halo mass. We will discuss the possible biases of this assumption in §6.

For central galaxies, we implement a model with considerably more flexibility. Because the the efficiency of star formation quenching for central galaxies may be halo mass dependent, the minimum mass scale for red central galaxies may be much higher than that for blue galaxies in a luminosity-threshold sample. Current models predict that this transition could be sharp (e.g., Croton et al. 2006; Dekel & Birnboim 2006; Cattaneo et al. 2006), or that it could be quite broad (e.g., Bower et al. 2006; Hopkins et al. 2008a; Somerville et al. 2008). At high redshift, massive halos may be more efficient at forming stars than in the present universe, thus a high fraction of high-mass halos may be blue (Dekel et al. 2008). We parameterize all these possibilities with a red central fraction of the form

$$f_{Rcen}(M) = f_{Rmax} \exp\left[\frac{-\beta\kappa M_{min}}{M - \beta M_{min}}\right] \quad (3)$$

when $M > \beta M_{min}$, and $f_{Rcen} = 0$ at lower masses. The parameter κ governs how sharp the transition is between halos hosting no central red galaxies and halos having an asymptotic probability of f_{Rmax} of having a red central galaxy. The

parameter β sets the overall shift in the mass scale for red central galaxies by setting the mass scale below which no halos host red central galaxies.

Figure 2 shows several examples of the red occupation function, defined as $f_{Rcen} \times \langle N_{cen} \rangle_M$. The thick solid line shows an example of $\langle N_{cen} \rangle_M$, the central occupation function for all galaxies, for the UDS sample. M_{min} for this sample is roughly $10^{11.6} h^{-1} M_\odot$. The thin solid curve shows a model in which $(f_{Rmax}, \kappa, \beta) = (0.2, 0, 0.1)$, which yields a constant $f_{Rcen} = 0.2$ at all halo masses. A quantity of interest is the ratio of the average halo mass of a red central galaxy to the average halo mass of a blue central galaxy, defined as

$$\frac{M_{red}}{M_{blue}} = \frac{n_{Rcen}^{-1} \int dM M n(M) f_{Rcen} \times \langle N_{cen} \rangle_M}{n_{Bcen}^{-1} \int dM M n(M) (1 - f_{Rcen}) \times \langle N_{cen} \rangle_M} \quad (4)$$

where $n(M)$ is the halo mass function, and n_{Rcen} and n_{Bcen} are the number density of red and blue central galaxies, respectively, that are calculated from the HOD by, eg,

$$n_{Rcen} = \int dM n(M) f_{Rcen} \times \langle N_{cen} \rangle_M. \quad (5)$$

For the thin solid curve, $M_{red}/M_{blue} = 1$ by definition. Red central galaxies are essentially a random subset of all central galaxies. The dotted curve shows a model in which $(f_{Rmax}, \kappa, \beta) = (0.75, 24, 0.75)$. This model produces a very broad transition between halos having a negligible probability of containing a red central galaxy to central galaxies being majority red. The number density of red centrals is the same as the solid curve, but now the mass ratio between red and blue central galaxies is 3.1. This function would represent a merger-induced red central model. The dashed curve shows a model in which $(f_{Rmax}, \kappa, \beta) = (0.8, 0.057, 2.5)$. In this model,

the transition between blue and red central galaxies is nearly instantaneous at $M = 2.5M_{\min}$. Once again, n_{Rcen} is the same as in the previous two models, but $M_{\text{red}}/M_{\text{blue}}$ is increased to 4.6. A function of this form represents the critical mass scale scenario.

3.3. Calculating Observables with the Model

To calculate the galaxy autocorrelation function, $\xi(r)$, from a given HOD, we use the analytic model described in the Appendix of Tinker et al. (2005) (see also Zheng 2004). As a brief description, the correlation function is broken into two parts: a one-halo term in which pairs of galaxies reside within a single halo, and a two-halo term in which pairs come from two distinct halos. The one-halo term dominates the correlation function at separations $r \lesssim 1 h^{-1} \text{Mpc}$, while the two-halo term contributes nearly all pairs at $r \gtrsim 1 h^{-1} \text{Mpc}$. The shape of the one-halo term is influenced by the radial distribution of satellite galaxies, which we assume to be the same as the dark matter. Specifically, we use the halo concentration-mass relation from Zhao et al. (2008). More importantly, the one-halo term is sensitive to the overall fraction of galaxies that are satellites (see the discussions in Zheng et al. 2008 and Tinker et al. 2009a). The satellite fraction is influenced both by the shape of the mass function and the form of the HOD. More satellites will increase the large-scale bias of a sample, but because the number of satellite-satellite pairs within a single halo increase as $\langle N_{\text{sat}} \rangle_M^2$, the effect of the small-scale clustering is more dramatic. At large scales, the shape of the two halo term is the same as the linear matter correlation function. At intermediate scales, $r \lesssim 3 h^{-1} \text{Mpc}$, halo bias deviates from a simple linear approximation, and a scale-dependent term is required (Tinker et al. 2009b). When implementing the analytic model for $\xi(r)$, we use the halo mass function of Tinker et al. (2008a) and the halo bias function of Tinker et al. (2009b). We assume that a halo is defined to be a spherical object with a mean interior density 200 times the background density.

For the UDS, the angular correlation function, $w(\theta)$, is measured. This quantity is defined as

$$w(\theta) = \int dz N^2(z) \frac{dr}{dz} \int dx \xi \left(\sqrt{x^2 + r^2 \theta^2} \right), \quad (6)$$

where $N(z)$ is the normalized redshift distribution of the galaxy sample, r is the comoving radial distance at redshift z and $dr/dz = (c/H_0)/\sqrt{\Omega_m(1+z)^3 + \Omega_\Lambda}$. As stated in §2.1, we use the estimate of $N(z)$ from Williams et al. (2009) that incorporates photometric redshift errors.

For DEEP2, we calculate the projected correlation function,

$$w_p(r_p) = 2 \int_0^{\pi_{\max}} \xi(r_p, \pi) d\pi. \quad (7)$$

As mentioned in §2.2 we set $\pi_{\max} = 20 h^{-1} \text{Mpc}$, the same as in the measurements. For the one-halo term, $20 h^{-1} \text{Mpc}$ is sufficient to eliminate redshift-space effects, therefore we use the isotropic real-space one-halo term in equation (7). For the two-halo term, coherent infall is still a concern. We take this effect into account by using the linear theory model of Kaiser (1987) when calculating the two-halo term. Although linear theory is not a fully descriptive model of $\xi(r_p, \pi)$ at separations of a few $h^{-1} \text{Mpc}$, for a projected quantity like $w_p(r_p)$ we find that it compares well to galaxy mocks constructed from N-body simulations in which $w_p(r_p)$ is estimated with

$\pi_{\max} = 20$ enforced. See Hamilton (1998) and Hawkins et al. (2003) for a thorough discussion and application of the Kaiser (1987) model to an unparameterized correlation function.

Because the COMBO-17 data integrate to $\pi_{\max} = 20 h^{-1} \text{Mpc}$, the effect of redshift-space distortion is negligible. To calculate $w_p(r_p)$ for the COMBO-17 data, no accounting of redshift-space effects are required and we use the isotropic, real-space $\xi(r)$ in equation 7, and integrate along the line of site until convergence.

For each sample, we use the Monte Carlo Markov Chain (MCMC) method to probe the likelihood distribution of the full parameter space. We have six free parameters. The first two, M_{\min} and M_{sat} , specify $\langle N \rangle_M$ for the full sample of galaxies. We have one parameter, f_{Rsat} , to split the satellite galaxies into red and blue subsamples. The last three parameters, β , κ , and f_{Rmax} , determine the fraction of central galaxies that are red as a function of halo mass. These parameters specify not just $\xi(r)$ but also the abundance of blue and red galaxies. We minimize the total χ^2 of the model, which we obtain from the sum of the χ^2 for the red and blue clustering measurements and the χ^2 for the galaxy abundances. The best-fit parameters for each sample are given in Table 1.

4. RESULTS

4.1. Clustering in the UDS

Figure 3a shows the best-fit model against the $w(\theta)$ data, and Figure 3b shows the HOD for all galaxies and the quiescent subsample. The relative bias between the star-forming and quiescent galaxies is high enough that the best-fitting model is on the extreme edge of allowed parameter space; to increase the clustering of quiescent galaxies relative to the star-forming subsample, the best-fit f_{Rcen} rapidly rises from 0 to 1 at a ‘‘critical’’ mass threshold of $M = 10^{12.2} h^{-1} M_\odot$, yielding a halo mass ratio of red to blue centrals of $M_{\text{red}}/M_{\text{blue}} \sim 6$. Because of the high central mass ratio, the clustering amplitude of red galaxies is boosted significantly. This fact, along with the high fraction of centrals that are red, forces the fraction of red satellite galaxies down to $f_{\text{Rsat}} \sim 22\%$, which is lower than the overall red fraction of galaxies.

However, there is a strong degeneracy axis between $M_{\text{red}}/M_{\text{blue}}$ and f_{Rsat} . Because the number of satellites increases linearly with halo mass, increasing f_{Rsat} also increases the large-scale bias of red galaxies without any increase the halo mass scale of red central galaxies. This, combined with the large error bars on the data, make the constraints on the parameters of the HOD model weak. Within the 2σ confidence limit, a model in which $f_{\text{Rsat}} = 0.59$ and $M_{\text{red}}/M_{\text{blue}} = 1.01$ is acceptable. This model is shown with the dashed line in Figure 3b. We will discuss this degeneracy and its implications in more detail §5.

4.2. Bright galaxies in DEEP2

Figure 4 presents results for DEEP2 galaxies in the $M_B < -20.5$ sample. Figure 4a shows both the measured clustering signal and the best-fit HOD model. Figure 4b shows the HOD for both the full galaxy sample and the red subsample. At all scales, the clustering of red galaxies is higher relative to blue galaxies. However, the $w_p(\text{red})/w_p(\text{blue})$ ratio is significantly smaller than that found in lower redshift samples such as SDSS (Zehavi et al. 2005; Li et al. 2006) and 2dFGRS (Norberg et al. 2002; Madgwick et al. 2003). In fact, the increased clustering of red galaxies in the two-halo term is best accounted for by a model in which red central galaxies

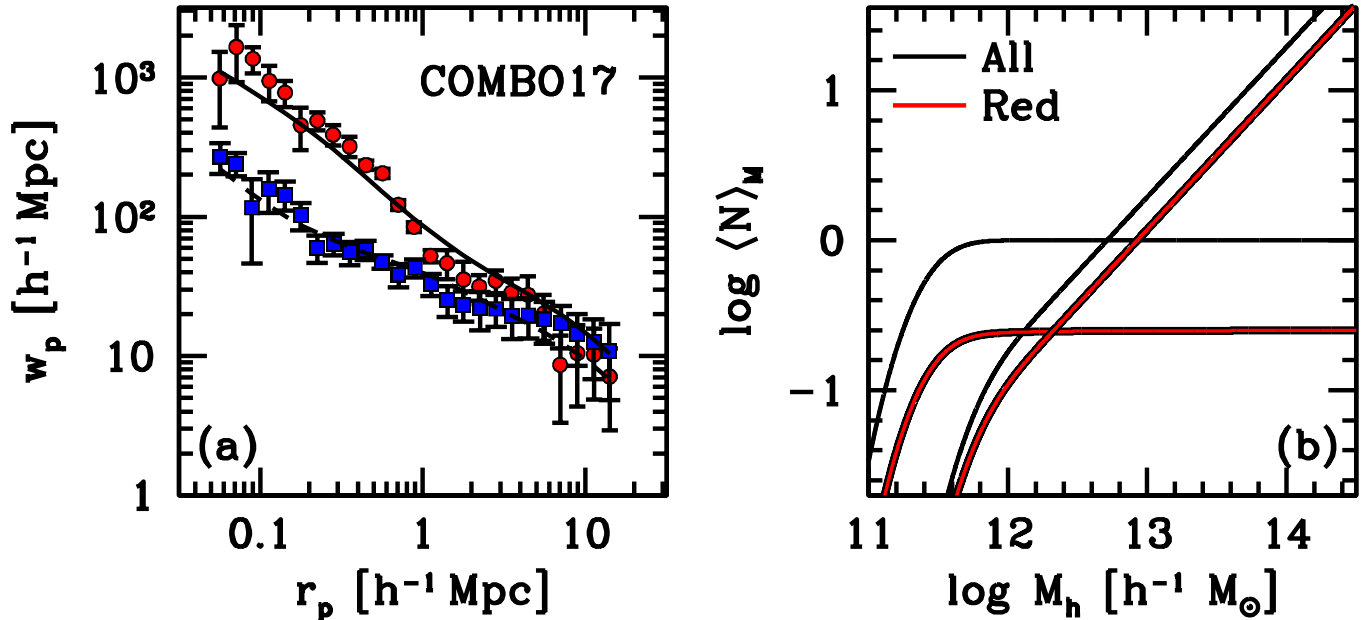


FIG. 6.— Panel (a): Measurements of the projected correlation function for galaxies in COMBO-17 by Phleps et al. (2006). The median redshift of the sample is $z \sim 0.6$. The circles and squares represent the measurements for red and blue galaxies, respectively. The solid and dashed curve represent the HOD model fits for red and blue galaxies, respectively. Panel (b): The best-fit occupation functions for all galaxies in the sample (thin solid curves) and red galaxies (thick curves). The halo mass ratio of red central galaxies, $M_{\text{red}}/M_{\text{blue}}$, is 1.27, in agreement with the results from both DEEP2 samples.

have no dependence on halo mass ($M_{\text{red}}/M_{\text{blue}} = 1.04$), but with a high fraction of satellite galaxies being red ($f_{\text{Rsat}} = 0.66$), twice the global fraction of red galaxies in this sample. Unlike the analysis of the UDS clustering, the constraints on the model parameters are strong.

The χ^2 value, at 64.4 for 29 degrees of freedom, is not ideal but we note that without a proper covariance matrix the χ^2 values are not fully robust. The χ^2 for the blue galaxies (39.1) is significantly larger than for the red (18.3). Visually, it appears that this is a result of the poor fit to the blue $w_p(r_p)$ in the one-halo term, but point-to-point scatter is also a concern; two points, the second and fourteenth, contribute a χ^2 of 22. To improve the fit at small scales, the amplitude of the one-halo term for both red galaxies and blue galaxies would need to increase. This is obtained by increasing the number of satellite galaxies, but it would come at the cost of increasing the amplitude of the large-scale bias as well. The best-fit model is somewhat above the data at large scales ($r_p \gtrsim 2 h^{-1} \text{Mpc}$), and increasing this disparity would decrease the quality of the fit (see also Wetzel & White 2009). Zheng et al. (2007), also using HOD modeling, produced fits that accurately reproduced the large-scale clustering of DEEP2 galaxies, but this result is due to the choice of cosmology: the WMAP1-type cosmology utilized in Zheng et al. (2007) has significantly less large scale power due its lack of tilt and higher matter density. We find that we are able to reproduce the Zheng et al. (2007) result when implementing the WMAP1 cosmology.

In this paper we are most interested in probing the halo mass scale at which star formation for red central galaxies becomes quenched, if there is one. Analysis of bright galaxies probes a higher halo mass scale, but this sample is useful for a number of reasons. First, it is a consistency check on the results obtained from the faint galaxies. Second, because the samples in Coil et al. (2008) are threshold samples, we know that the f_{Rcen} for the *faint* sample can never be lower than f_{Rcen}

for the *bright* sample at a given halo mass. It is also highly unlikely that f_{Rcen} for the fainter sample would be higher than that of the brighter sample at $M \gtrsim 10^{14} h^{-1} M_{\odot}$ unless magnitude errors were extreme. The bright sample is fully contained within the faint sample; the central galaxies in high-mass halos are the same galaxies that produce the clustering in the bright sample. Thus we fix the value of f_{Rmax} in the faint sample to be the best-fit value of from the $M_B < -20.5$ sample, 0.25, ensuring that f_{Rcen} for the faint sample will be the same as that in the bright sample in the overlapping halo mass range.

4.3. Faint galaxies in DEEP2

Figure 5a presents the clustering of $M_B < -19.5$ in DEEP2, along with the model with the lowest χ^2 from the MCMC chain. As with the bright galaxies, the clustering of red galaxies in this sample is stronger than that of the blue galaxies at all scales (the last three data points in the red $w_p(r_p)$ that have low amplitudes are most likely a result of sample variance), but the relative bias between red and blue samples at large scales is only moderately above unity (Coil et al. 2008 calculate a relative bias of 1.25). Thus, the best-fitting HOD in Figure 5b is similar to that of the bright galaxies; f_{Rcen} is nearly independent of halo mass, yielding $M_{\text{red}}/M_{\text{blue}} = 1.48$. The central occupation function for red galaxies contains a sharp cutoff at $M = 10^{11.4} h^{-1} M_{\odot}$, which is the feature that causes the value of $M_{\text{red}}/M_{\text{blue}}$ to be larger than one. This cutoff is required by the constraints on the number density rather than on the clustering; without such a cutoff, the space density of red galaxies would be too high. The fraction of satellites that are red is 52%, twice the overall red fraction of this sample.

Visually, the fit for this sample appears to match the data better than with the brighter sample, but the χ^2 is roughly the same, at 63.7 (although for one less degree of freedom because f_{Rmax} has now been fixed to 0.25). The larger num-

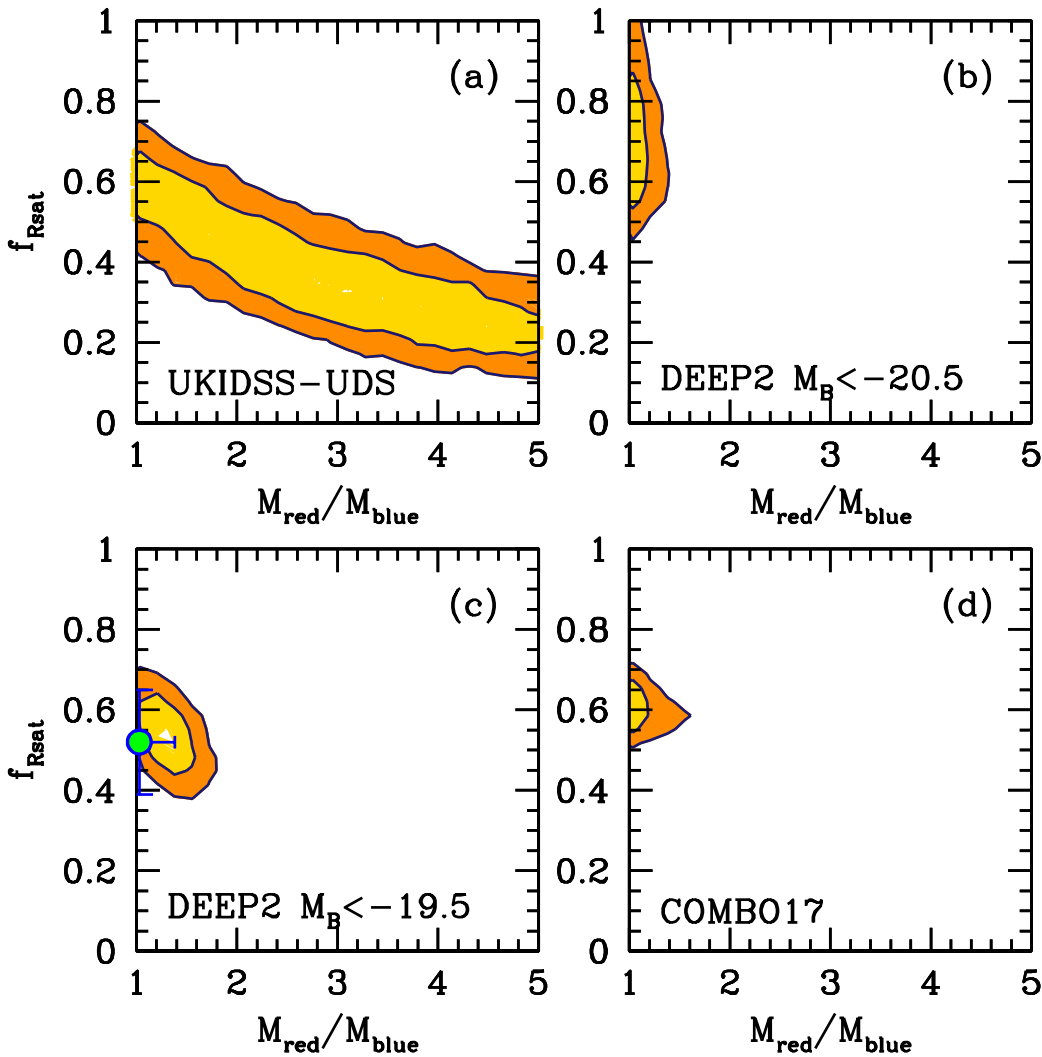


FIG. 7.— Constraints in the $M_{\text{red}}/M_{\text{blue}}-f_{\text{Rsat}}$ plane for the four samples analyzed in this paper. Contours represent 1- and 2- σ constraints. In panel (a), showing the constraints from the UDS clustering data, the degeneracy between the central mass ratio and the fraction of red satellites is clear. For the other three samples, $M_{\text{red}}/M_{\text{blue}}$ is consistent with unity, with a red satellites fraction of ~ 0.6 . In Panel (c), showing the constraints for the faint DEEP2 sample, the circle with errorbars represents the results of a model in which f_{Rmax} is allowed to be a free parameter. In the contours, $f_{\text{Rmax}} = 0.25$ to agree with the results from the bright DEEP2 sample. Errorbars are 2σ .

ber density of this sample yields smaller error bars in the 1-halo term, and once again point-to-point variance is larger than the errors for several data points: two data points account for 27% of the total χ^2 . When using the WMAP1 cosmology to model the red and blue, the χ^2 of the fit is 28.9 (yielding $\chi^2/\nu = 0.93$), a significant improvement on the results discussed above. However, the constraints on f_{Rsat} and $M_{\text{red}}/M_{\text{blue}}$ are unchanged. An additional difference between the Zheng et al. (2007) analysis and that of this paper is the freedom in α_{sat} . We will discuss this in more detail in §6.

As a check on these results, we have performed the HOD analysis of the faint sample without the prior on f_{Rmax} obtained from the analysis of the bright sample. The results are consistent within their 1- σ contours, which we will show in Figure 7. In this test, f_{Rsat} was nearly unchanged, while the best-fit $M_{\text{red}}/M_{\text{blue}}$ decreased to be 1.0, the same as for the

bright galaxies. The best-fit value of f_{Rmax} is 0.16, rather than 0.25, which removes the need for the sharp cutoff in f_{Rcen} at $10^{11.4} h^{-1} M_{\odot}$ in order to match the number density.

4.4. Clustering Analysis for COMBO-17

Figure 6a and 6b show the clustering results from COMBO-17 and the resulting halo occupation functions, respectively. The $w_p(r_p)$ measurements for red and blue galaxies are similar to those in DEEP2; at small scales, the clustering of red galaxies is strongly enhanced relative to blue galaxies, but in the two-halo term the difference in the clustering is minimal, with sample variance muddling the comparison at $r_p \gtrsim 10 h^{-1} \text{Mpc}$. This results in a best-fit HOD that is the same as those found in the DEEP2 sample; $M_{\text{red}}/M_{\text{blue}} = 1.01$ and $f_{\text{Rsat}} = 0.58$, which is more than twice as high as the overall red fraction of the sample.

The reduced χ^2 value of the best fit model is 1.9. The χ^2 for

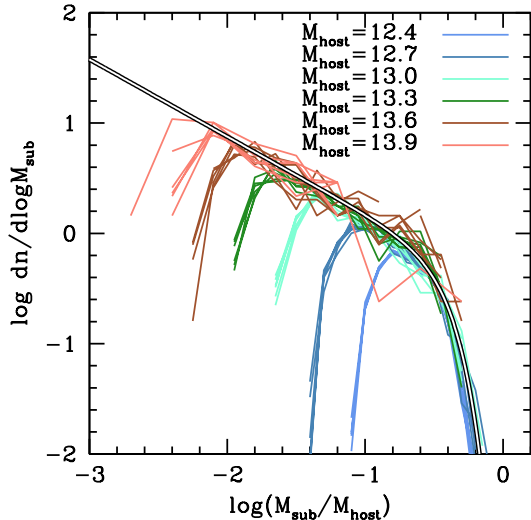


FIG. 8.— The subhalo mass function from a numerical simulation presented in Wetzel & White (2009). Here M_{sub} is the mass of the subhalo at the time of accretion. The thin curves represent the N-body results, while the thick curve is the fitting function given in Equation (10). For the numerical results, each color represents a different host halo mass bin, ranging from $\log M_{\text{host}} = 12.4$ to $\log M_{\text{host}} = 13.9$. For each bin in M_{host} , the six lines show results for six redshift outputs ranging from $z = 0.8$ to $z = 1.6$. The turnover at low $M_{\text{sub}}/M_{\text{host}}$ for each mass bin is due to the fixed particle limit in the subhalo catalog; we use only subhalos with more than 2000 particles at infall to avoid artificial numerical disruption. The overlapping results for each mass bin show that the subhalo mass function is universal over a wide range of halo mass and redshift.

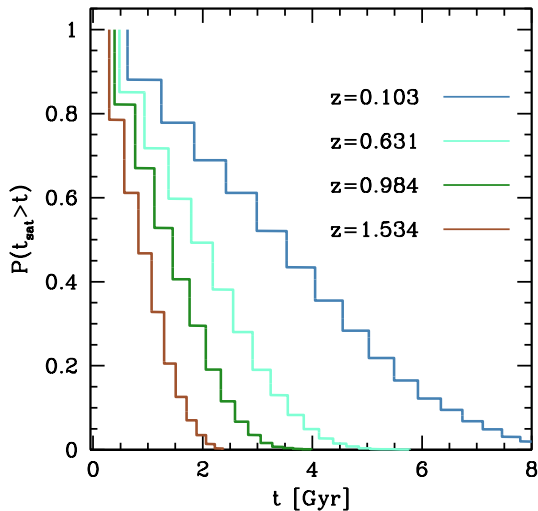


FIG. 9.— The distribution of subhalo ages, defined as the time since a subhalo was accreted onto its parent halo. Results are from the simulations of Wetzel & White (2009). The y-axis indicates the fraction of subhalos with accretion times longer than the value t . As redshift increases, the mean age of a subhalo becomes younger because dynamical friction is more efficient at higher redshifts due to the higher density of most halos. The halo catalogs span the redshift range $z = 0$ to $z = 1.6$, but in this plot we show only four output redshifts to avoid crowding.

the blue $w_p(r_p)$ is 14.7 for 25 data points. The source of the high χ^2 is localized to the transition region between 1-halo and 2-halo clustering in the red $w_p(r_p)$; half of the total χ^2 value is accrued between $0.5 < r_p < 1.1$, where the clustering amplitude drops rapidly. P06 have also performed HOD anal-

ysis of these data, obtaining a much better χ^2 value than that found here, 35.9 versus 88.3. There are several reasons for the lower χ^2 value from the P06 analysis. First, P06 have a different cosmological model with no tilt, which reduces the large-scale power. Second, P06 leave σ_8 as a free parameter, increasing the freedom of their cosmological model. This parameter is left free for *both* the red and blue subsamples, yielding best-fit values of σ_8 of 0.84 ± 0.08 and 1.19 ± 0.09 for the red and blue subsamples, respectively. The lower σ_8 value for the red model fit is required by the low relative bias of blue and red galaxies in the data. Third, and most important, P06 implement a physically unrealistic HOD model. P06 assume the same form of the HOD for both blue and red subsamples: a power-law in which $\langle N \rangle_M = (M/M_0)^\beta$ for $M > M_0$. The power-law index β is left as a free parameter. This model is unrealistic in that it does not reproduce known aspects of halo occupation parameterized in equations (1) and (2): a self-consistent separation of central and satellite galaxies; a “shoulder” in $\langle N \rangle_M$ in the halo mass range between M_{min} and M_{sat} (nearly a factor of 20 in halo mass), in which the scatter in $\langle N \rangle_M$ is sub-Poisson because satellites are a minority of the galaxies. Lastly, when modeling the red and blue galaxies separately, P06 does not require that the number of central red galaxies and central blue galaxies be ≤ 1 at fixed halo mass. P06 stipulate that if $\langle N \rangle_M > 1$, the “first” galaxy is central and the remaining objects are satellites. However, this is done for *both* red and blue occupation functions. The implication is that there are *two* central galaxies per halo, one red and one blue, above $M_{0,\text{red}}$. When implementing an HOD that is similar to equations (1) and (2), P06 see no difference in the χ^2 for the blue galaxies, but the χ^2 for the red galaxies increases by 20. See Tinker et al. (2009a) for a full discussion of the implications of an HOD model of the type utilized by P06.

4.5. Parameter Constraints for All the Samples

Figure 7 shows the constraints in the $M_{\text{red}}/M_{\text{blue}} - f_{\text{Rsat}}$ plane. The x-axis does not extend below $M_{\text{red}}/M_{\text{blue}} = 1$ because that is the minimum value allowed from equation (3). For the UDS data, the lack of significant constraints is clear from the strong degeneracy between f_{Rsat} and $M_{\text{red}}/M_{\text{blue}}$; with a larger fraction of red satellite galaxies, the need for a large ratio between the masses of red and blue central galaxies is reduced. This is a consequence of the small volume of the sample and the use of angular clustering.

For the next three samples, the results are markedly different. All of the samples are consistent, within the $1-\sigma$ constraints, with red central galaxies being a random subsample of all central galaxies. A value of $M_{\text{red}}/M_{\text{blue}} = 2$ is excluded at more than $2-\sigma$ for all the samples. The fraction of red satellite galaxies is high, being consistent with 60% in all samples. Note that $f_{\text{Rsat}} = 0.6$ is consistent with the results from the UDS data, in which case $M_{\text{red}}/M_{\text{blue}} \approx 1$. Thus, if there is no strong evolution in the red satellite fraction from $z \approx 0.9$ to 1.4, the UDS data also suggest that red central galaxies are a random subsample of all galaxies.

5. THE TIMESCALE FOR SATELLITE TRANSFORMATION

5.1. A Simple Model

Galaxies form within dark matter halos; the halo occupation formalism is built upon this concept. High resolution collisionless N-body simulations track dark matter halos after they have been accreted onto larger halos. Models that associate these *subhalos* with the satellite galaxies that con-

TABLE 1
PARAMETERS FOR BEST-FIT MODELS

Sample	f_{Rsat}	f_{Rmax}	κ	$\log M_{\text{sat}}$	$\log \beta$	$\log M_{\text{min}}$	n_{red}	n_{blue}	ν	χ^2
UDS	0.22	0.98	2.47	12.803	-1.815	11.838	1.10×10^{-3}	3.17×10^{-3}	19	10.8
DEEP2 -20.5	0.66	0.25	0.04	13.365	-0.363	11.882	8.46×10^{-4}	2.13×10^{-3}	29	64.4
DEEP2 -19.5	0.52	0.25	0.45	12.800	-1.891	11.682	2.37×10^{-3}	8.00×10^{-3}	30	63.7
COMBO-17	0.59	0.17	0.13	12.694	0.050	11.391	3.96×10^{-3}	1.23×10^{-2}	46	86.1

NOTE. — The units of M_{min} and M_{sat} are $h^{-1} M_{\odot}$. ν is the number of degrees of freedom in the sample.

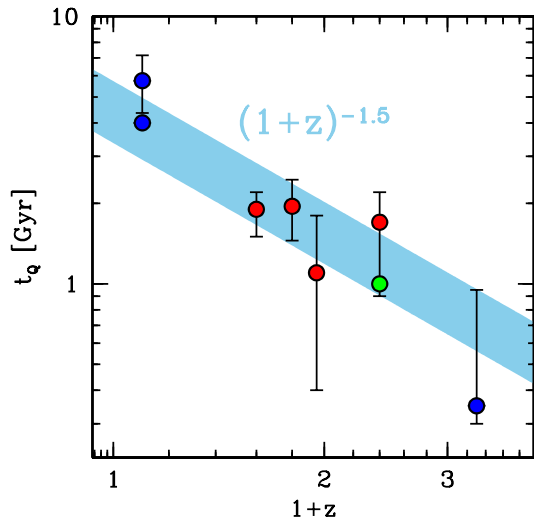


FIG. 10.— Timescale for galaxies to transition from blue to red, or from star-forming to quiescent. All error bars are 2σ . The middle four (red) data points represent, in order of increasing redshift, COMBO-17, DEEP2 faint, DEEP2 bright, and the UDS. The blue data points are taken from other papers. The datum at $z = 2.3$ is from the Tinker et al. (2009a) analysis of the clustering of DRGs. The upper datum at $z = 0.1$ is from Wang et al. (2007), in which the exponential decay of star formation in satellites was constrained to be 2.5 Gyr. We assume that satellites are “quenched” when the star formation rate decreases by a factor of 10, or 2.3 e-folding times. The lower datum at $z = 0.1$ is an estimate of the timescale for transitioning to the red sequence using the clustering data and analysis in Zehavi et al. (2005). The green circle at $z = 1.4$ is the quenching timescale inferred from the UDS data if we assume that $M_{\text{red}}/M_{\text{blue}} = 1$, in agreement with the other three samples. The shaded band is a power-law in which the quenching timescale varies with the dynamical time of dark matter halos, $(1+z)^{-1.5}$.

stitute groups and clusters have been successful at reproducing measured clustering of galaxies at various redshifts (e.g., Kravtsov et al. 2004; Conroy et al. 2006; Wang et al. 2006, 2007; Marín et al. 2008; Moster et al. 2009; Wetzel & White 2009). In these models, the known unknown is the exact relationship between halo and subhalo mass and the luminosity (or other galaxy properties, such as stellar mass) of the galaxy. A simple and successful approach has been to assume a monotonic relationship between galaxy luminosity and halo mass, where the exact functional form of the mass-to-light ratio is constrained to match the luminosity function of galaxies. Although there is known to be some scatter in halo mass at fixed galaxy properties (More et al. 2009), this monotonic approach has proved successful and useful in myriad studies, producing results quantitatively similar to those that incorporate scatter.

In the results in §4, we have made no assumptions about

the population of dark matter subhalos within distinct halos. We have also made few assumptions about the M/L ratio as a function of halo mass because the samples we have analyzed have are defined with a threshold luminosity, rather than being broken into multiple luminosity bins. However, to make inferences about the evolution of satellite galaxies we must make use of N-body simulations that keep track of merger rates and the lifetimes of subhalos. For each observational sample, we have determined the total number of satellite galaxies in each halo, as well as the fraction of those galaxies that are classified as red or quenched. To determine the quenching time of a galaxy once it is accreted, a simple approach is to consider all subhalos in a given halo that contain galaxies in the sample. Using the monotonic M/L ratio, this would simply be the $\langle N_{\text{sat}} \rangle_M$ most massive subhalos (where the subhalos are ranked by their mass *at the time of accretion*, not their present-day mass, which is affected by orbit-dependent tidal stripping; see, e.g., Conroy et al. 2006; Moster et al. 2009; Wetzel & White 2009). These subhalos are then ranked by the time elapsed between accretion and the redshift of observation. Assuming that the oldest subhalos are the ones that have had their star formation quenched and migrated to the red sequence, the value of f_{Rsat} sets the quenching timescale.

One complication is that some satellite galaxies may have been red *before* they became satellites. The results from all the samples in §3 indicate that, even at low halo masses, the fraction of field red galaxies is 20-30%. The mechanism by which these galaxies transitioned to the red sequence is unrelated to ram-pressure stripping or tidal stripping. A model in which field red galaxies are quenched by tidal interactions with nearby massive structures is also disfavored; an environmentally-dependent quenching mechanism of this type would enhance the large-scale clustering of red galaxies. We have already noted that the relative bias of red to blue galaxies is difficult to match even if the probability of a central galaxy being red is independent of environment. An environmentally-dependent f_{Rcen} is also disfavored at $z = 0$ (Tinker et al. 2008b).

To remove the contribution of satellite galaxies that were red before accretion, we determine the quenched fraction of satellite galaxies, f_Q , by

$$f_Q = \frac{f_{\text{Rsat}} \bar{n}_{\text{sat}} - \bar{n}_{\text{prev}}}{\bar{n}_{\text{sat}} - \bar{n}_{\text{prev}}}, \quad (8)$$

where \bar{n}_{sat} is the number density of satellites and \bar{n}_{prev} is the number density of previously quenched satellites, given by

$$\bar{n}_{\text{prev}} = \int dM n(M) \int dM_{\text{sub}} n_{\text{sub}}(M_{\text{sub}}|M) f_{\text{Rcen}}(M_{\text{sub}}) \times \langle N_{\text{cen}} \rangle_{M_{\text{sub}}} \quad (9)$$

where $n_{\text{sub}}(M_{\text{sub}}|M)$ is the subhalo mass function (where once again M_{sub} is defined as the mass at the time of accretion), and $f_{\text{Rcen}}(M_{\text{sub}})$ is the central red fraction determined for each sample. Note that $n_{\text{sub}}(M_{\text{sub}}|M)$, in our definition, does not have units of volume but rather is the number of subhalos within a given parent halo of mass M . We will describe our fitting function for this quantity in the following subsection. Here, we assume that the central galaxy red fraction does not strongly evolve since the time of satellite accretion, supported by the mild evolution in f_{Rcen} across samples of §3. Equation (8) yields a quenched fraction that is somewhat smaller than the overall red fraction. For three of the four samples, f_{Rcen} is nearly independent of mass and $\bar{n}_{\text{prev}} \approx f_{\text{Rmax}} \bar{n}_{\text{sat}}$. For the best-fit model obtained for the UDS, f_{Rcen} depends strongly on mass. However, in this model, the difference between f_{Rsat} and f_{Q} is minimal; in that particular model, $f_{\text{Rcen}} = 0$ below $M \sim 10^{12.2} h^{-1} M_{\odot}$. Most satellites in this sample are below this mass, thus the fraction of subhalos that became red before accretion is small. Recall, however, that the constraints on f_{Rcen} in the UDS are broad.

5.2. N-body Simulations

To implement the model in the previous subsection, we require two quantities: the subhalo mass function and the distribution of accretion times for subhalos. We use the halo and subhalo catalogs from the high-resolution N-body simulation analyzed in Wetzel & White (2009). The simulation is of the same cosmology as that assumed here. The volume of the simulation is $200 h^{-1} \text{Mpc}$ per side, containing 1500^3 particles, with a particle mass of $1.6 \times 10^8 h^{-1} M_{\odot}$ and a force resolution of $3 h^{-1} \text{kpc}$. Halos are identified using the friends-of-friends halo finding algorithm with a linking length of 0.168 times the mean interparticle separation. Halos defined in this way have different masses than halos defined by $\Delta = 200$ (White 2002; Tinker et al. 2008a), as done in all analytic calculations in this paper. We convert from FOF mass to $\Delta = 200$ mass with a factor of 1.3. See Wetzel et al. (2009) and Wetzel & White (2009) for details of subhalo finding and tracking.

Figure 8 shows the results for the subhalo mass function at six different redshifts between $z = 0.9$ and $z = 1.6$. The results are plotted as a function of $M_{\text{sub}}/M_{\text{host}}$, in which units $dN/d \ln M_{\text{sub}}$ is independent of host halo mass. This self-similarity of the subhalo mass function has been shown before for subhalo masses measured at a fixed redshift (e.g., Gao et al. 2004; De Lucia et al. 2004; Kravtsov et al. 2004; Wetzel et al. 2009), but note that M_{sub} here is the mass at the time of accretion, the quantity that correlates with the observational properties of the galaxy contained within them. Figure 8 also demonstrates that the subhalo mass function changes little with redshift. For each bin in M_{host} , the N-body data turn over at low mass ratios. This is due to the finite particle number in the subhalo catalogs utilized; subhalos of the same initial mass will experience differential tidal forces. This causes some subhalos to drop below the particle limit of the subhalo catalog, thus the downturn is artificial. The region where the curves overlap is the true subhalo mass function. We use a fitting function of the form

$$\frac{dN}{d \ln M_{\text{sub}}} = 0.13 \left(\frac{M_{\text{sub}}}{M_{\text{host}}} \right)^{-0.7} \exp \left[-9.9 \left(\frac{M_{\text{sub}}}{M_{\text{host}}} \right)^{2.5} \right] \quad (10)$$

when calculating equation (9).

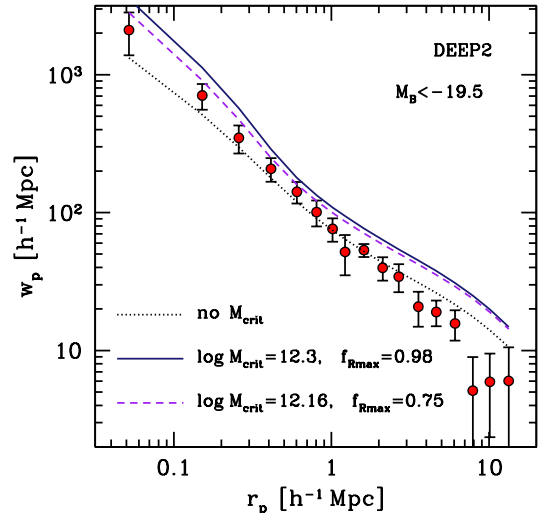


FIG. 11.— The effect of imparting a critical mass scale of f_{Rcen} for the faint red DEEP2 sample. The dotted curve is the model fit from Figure 5. The solid curve is the resulting correlation function from a model in which red galaxies rapidly dominate the central galaxy population above the critical mass obtained in the shock-heating model of Dekel & Birnboim (2006). The value of $M_{\text{red}}/M_{\text{blue}}$ is 10 in this model. The dashed curve is a less extreme model in which the majority of galaxies are red above the critical mass. For this model, $M_{\text{red}}/M_{\text{blue}} = 5$.

Figure 9 shows the age distribution of subhalos at three different redshifts. The y-axis is the cumulative distribution of satellites sorted by the time since they were accreted. The value on the y-axis indicates the fraction of subhalos that were accreted more than time t ago at each redshift. We define t_{sat} as $t - t(\text{accretion})$, and $t(\text{accretion})$ is defined as the time at which a subhalo is first linked to its parent halo by the FOF halo finder. The shape of $P(t_{\text{sat}} > t)$ clearly depends on redshift; at earlier epochs, halo densities are higher by $(1+z)^3$, thus the dynamical timescale decreases by $(1+z)^{-1.5}$. Once the quenched fraction of satellites is determined, the quenching timescale, t_{Q} found by smoothly interpolating between the numerical data in the $P(t_{\text{sat}} > t)$ distribution. We determine t_{Q} at the median redshift of each sample. In tests with the UDS sample, we find negligible differences between calculating t_{Q} at the median redshift and using the full $N(z)$ of the sample.

5.3. Results

Figure 10 shows the results of the model described in §5.2 for all four samples (middle four points), with 2σ error bars shown. All four samples are consistent with a value of $t_{\text{Q}} \sim 1.8 \text{ Gyr}$. There is no obvious dependence on redshift within these four samples. Figure 10 also shows quenching times from higher and lower redshift obtained from the literature. At $z \sim 2.3$, Tinker et al. (2009a) have analyzed the clustering of distant red galaxies (DRGs). These are massive galaxies that reside in halos with $M_{\text{min}} \approx 10^{12} h^{-1} M_{\odot}$. Some fraction of these galaxies have highly attenuated star formation rates, enough to be classified as red-and-dead (Labbé et al. 2005; Papovich et al. 2006; Kriek et al. 2006). Tinker et al. (2009a) found that the fraction of satellite galaxies that must be DRGs is between 0.5 and 1 (2σ), while current estimates put the fraction of DRGs that are quenched between 10-30% (Labbé et al. 2005; Papovich et al. 2006). Using these errors and the model described above, the quenching time for these

galaxies is between 300 and 950 Myr (2σ).

At low redshift, current estimates for the quenching timescale of satellite galaxies are much longer. Wang et al. (2007) used the clustering of star-forming and quiescent galaxies, as defined by the D_n4000 break in the galaxy spectrum (e.g., Kauffmann et al. 2003a), to determine the quenching timescale of satellite galaxies in the SDSS. They found an e -folding time for the star formation rate of satellite galaxies of 2.5 Gyr. Setting the quenching time to be the time at which a galaxy’s star formation rate is attenuated by a factor of 10, we find $t_Q = 5.75$ Gyr. This factor of 10 is roughly the difference between the star-forming and quiescent samples in the UDS (W09), as well as the blue and red subsamples in DEEP2 (Noeske et al. 2007). Although Wang et al. (2006) provide no formal error estimate on this number, a rough error bar is 25%.

The blue circle at $z = 0.1$ is the quenching time we determine through the clustering analysis of Zehavi et al. (2005), who use HOD modeling of color-selected samples in the SDSS to determine the red satellite fraction and the red central fraction of galaxies. For galaxies in magnitude bins centered on $M_r = -19.5$ and $M_r = -20.5$, the model in section §5.1 yields quenching times of ~ 4 Gyr. This estimate is meant to be a consistency check on the Wang et al. (2006) results; a more thorough analysis of the final data release of SDSS galaxies using these techniques will be presented by Wetzel et al. (in preparation). The green circle at $z = 1.4$ is the quenching time obtained if we impose a prior of $M_{\text{red}}/M_{\text{blue}} \leq 1.1$ on the MCMC analysis of the UDS clustering. Such a prior increases the fraction of satellites that are red in order to match the clustering amplitude of red galaxies, thus decreasing the quenching time.

The shaded band in Figure 10 is a power-law that goes as $(1+z)^{-1.5}$, following the redshift dependence of the dynamical time of dark matter halos. From $z = 0$ to $z = 2.3$, the results are consistent with a quenching timescale that is proportional both to the dark matter halo dynamical time and the satellite infall time.

6. DISCUSSION

6.1. How do Central Galaxies Arrive on the Red Sequence?

The majority of galaxies in the universe are central galaxies. As discussed in the introduction, current theories on the buildup of the red sequence focus on how to transform these central galaxies from star-forming objects to quiescent, red-and-dead objects. One set of ideas posits that there is a critical halo mass at which star formation is quenched, either from AGN heating or through sustainable shock heating (eg, Croton et al. 2006; Dekel & Birnboim 2006). This theory of a critical halo mass is clearly at odds with the clustering results analyzed here. If there exists a sharp critical mass scale above which galaxies become red, the relative clustering of red and blue galaxies would be significantly higher than that observed.

Figure 11 demonstrates this point quantitatively. The clustering data for the red galaxies in the faint DEEP2 sample are shown with the best-fit model from Figure 5. The solid curve is a model in which the fraction of red central galaxies transitions from 0 to 1 sharply at $M_{\text{crit}} = 2 \times 10^{12} h^{-1} M_{\odot}$, yielding $M_{\text{red}}/M_{\text{blue}} = 10$. The shape of f_{Rcen} is similar to the dashed curve from Figure 2. To keep the number density fixed at the observed number density of red galaxies, f_{Rsat} is reduced from 0.6 to 0.45. But even with the lower satellite fraction in this new model, the amplitude of clustering is significantly higher

than the data. The dashed curve shows the results for a less extreme model with a lower M_{crit} and $f_{\text{Rmax}} = 0.75$, yielding $M_{\text{red}}/M_{\text{blue}} = 5$. This model is in better agreement with the data in the one-halo term, but is just as discrepant in the two-halo term. This type of model also fails for the bright DEEP2 sample as well as the COMBO-17 data. For the UDS, a hard critical threshold is the best-fit model (cf, Figure 3), but the errors are too large to distinguish between this model and one in which $M_{\text{red}}/M_{\text{blue}} = 1$.

The ‘secular’ scenario (Bower et al. 2006), where instead of a critical halo mass threshold, there is a critical *galaxy* mass threshold, also predicts a strong dependence of f_{Rcen} on halo mass. At $M = 10^{11.3} h^{-1} M_{\odot}$, $f_{\text{Rcen}} \sim 0$, and by $M = 10^{12.0} h^{-1} M_{\odot}$ the fraction of red central galaxies is near unity (see Figure 6 in Hopkins et al. 2008a). The merger scenario has a weaker dependence of f_{Rcen} on M , but still produces a high $M_{\text{red}}/M_{\text{blue}}$ ratio. The *halo* merger rate depends little on halo mass (Cohn et al. 2001; Fakhouri & Ma 2007). This is also true of the merger rate of subhalos with host halos, which should more accurately track the galaxy merger rate (Wetzel et al. 2009). However, the mapping between halo mass and galaxy mass is complex; the M_{gal}/M ratio peaks at $M \sim 10^{12} h^{-1} M_{\odot}$ and falls off as a power law at higher and lower halo masses (see, eg, Wang et al. 2007; Conroy & Wechsler 2009; Moster et al. 2009). Because $M_{\text{gal}} \sim M^{0.4}$ at $M \gtrsim 10^{12} h^{-1} M_{\odot}$, a 10:1 halo-halo minor merger can contain galaxies with mass ratios of 3:1, yielding a major galaxy merger (Hopkins et al. 2008a; Maller 2008). In all calculations below we use the redshift-dependent stellar mass functions of Marchesini et al. (2007) assign stellar masses to halos and subhalos using abundance matching, interpolating between redshifts to obtain the stellar mass function at the redshift of a given sample.

Figure 12 shows the $z = 1.5$ red central fraction induced by major mergers, which we define as stellar mass ratios of 3:1 or closer, that have occurred over the previous Gyr. The small circles indicate the fraction of *halos* that have experienced a halo-subhalo (central-satellite) merger with mass ratios smaller than 2:1, 3:1, and 5:1, respectively, from the simulations of Wetzel et al. (2009). The lack of strong dependence on halo mass is clear. Using abundance matching to map halo mass onto galaxy mass, a 3:1 mass ratio for *galaxies* in those same halos yields a red central fraction of $\sim 10\%$ at $M = 10^{12} h^{-1} M_{\odot}$, rising to $\sim 30\%$ at $10^{13} h^{-1} M_{\odot}$ and $\sim 60\%$ at $10^{14} h^{-1} M_{\odot}$. The right hand panel of Figure 12 compares the central occupation function for red galaxies for model with $M_{\text{red}}/M_{\text{blue}} = 1$ to $\langle N_{\text{cen}} \rangle_M$ created by the merger scenario. At $z = 1.5$, the merger scenario yields a central galaxy number density that is too low by roughly a factor of 3. As stated above, the halo merger rates are calculated using a lookback time of 1 Gyr. Increasing this timescale increases the fraction of halos that have experienced mergers, but it does not change the *shape* of the merged fraction with halo mass, thus we consider the amplitude of this function to be a free parameter set by the overall number of red galaxies. Using the 1 Gyr lookback time to calculate f_{merge} , the merger scenario yields $M_{\text{red}}/M_{\text{blue}} = 2.2$. Increasing the normalization of f_{merge} to produce the correct number density of yields $M_{\text{red}}/M_{\text{blue}} = 2.9$. These values are in agreement with the weak constraints on f_{Rcen} shown in Figure 7. At $z = 0.8$, the redshift of the faint DEEP2 sample, the merger scenario yields $M_{\text{red}}/M_{\text{blue}} = 3.8$ using the 1 Gyr lookback time, and it yields $M_{\text{red}}/M_{\text{blue}} = 5.2$ if the amplitude of f_{merge} is increased

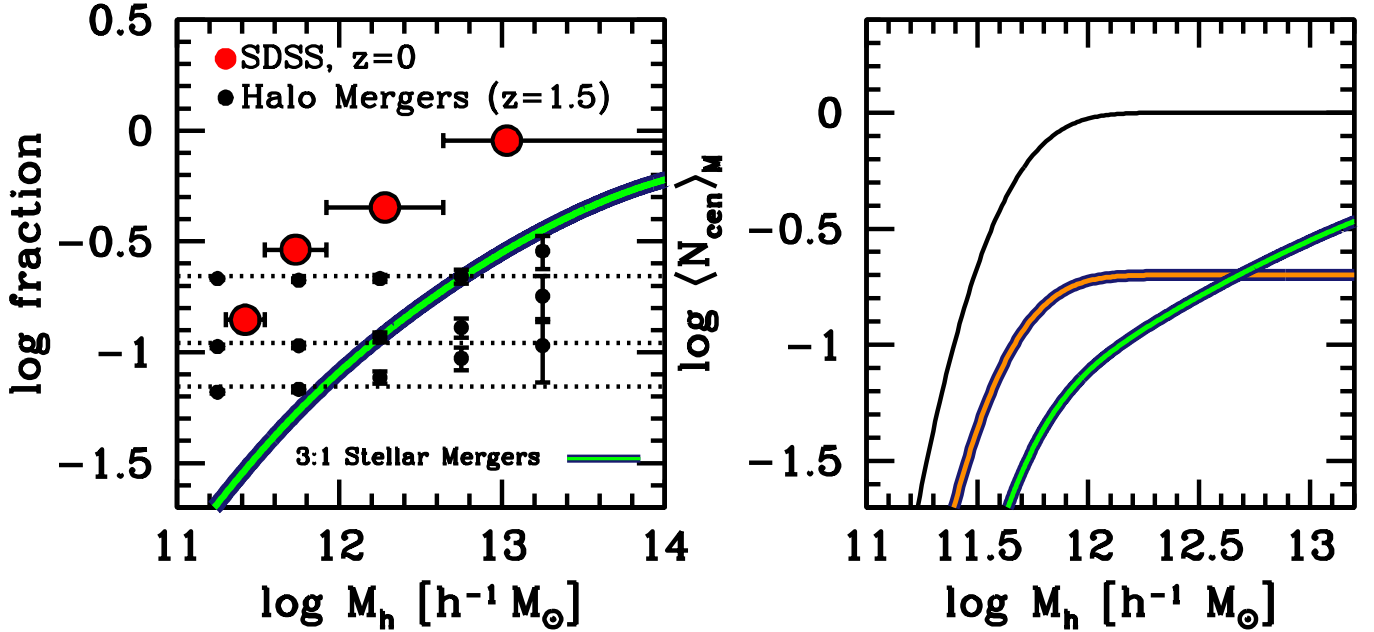


FIG. 12.— *Left Panel*: Small circles with errors represent the fraction of halos that have experienced a halo-subhalo (central-satellite) merger within the last Gyr with mass ratios smaller than 5:1 (*upper*), 3:1 (*middle*), and 2:1 (*lower*). The dotted lines show the mean values as for each mass ratio limit. The thick solid curve shows the fraction of halos whose central galaxy has experienced a merger with a stellar mass ratio smaller than 3:1. The large red circles represent the fraction of red central galaxies from Zehavi et al. (2005) analysis of SDSS galaxy clustering. *Right Panel*: Central occupation functions. The thin solid curve represents $\langle N_{\text{cen}} \rangle_M$ for the full UDS sample. The thick red line represents a model with $M_{\text{red}}/M_{\text{blue}} = 1$. The thick green line represents $\langle N_{\text{cen}} \rangle_M$ produced by the merger scenario.

to produce the proper red central number density. The higher values reflect the change in the halo mass function; under the merger scenario most high-mass halos are quenched, and the abundance of high-mass halos has increased substantively from $z = 1.4$ to $z = 0.8$. Results for COMBO-17 are similar. These values are strongly excluded for both the DEEP2 and COMBO-17 results. Thus, while the UDS data are broadly consistent with the merger scenario, DEEP2 and COMBO-17 are not.

To connect with the low redshift universe, Figure 12 also shows the dependence of f_{Rcen} on halo mass obtained from SDSS clustering by Zehavi et al. (2005). The shape of f_{Rcen} at $z = 0.1$ is consistent with the merger scenario (see also Hopkins et al. 2008a). If the COMBO-17 results are representative of the clustering of blue and red galaxies at $z = 0.6$, what occurs from $z = 0.6$ to $z = 0$ to induce the change in f_{Rcen} ? Selection effects seem unlikely to impart a mass dependence in f_{Rcen} in SDSS; indeed, the results of Maller et al. (2009) demonstrate that many low-luminosity galaxies in SDSS are misclassified as red due to dust effects. Similarly, selection biases seem unlikely to *remove* a mass dependence in f_{Rcen} in COMBO-17 and DEEP2. Red galaxies are selected by different methods in these two samples; for COMBO-17, spectral energy distribution fitting is used; in DEEP2, a color cut similar to SDSS is employed.

Is there evolution in the mechanism by which central galaxies quench their star formation? For halos of $\lesssim 10^{11.5} h^{-1} M_\odot$, the red central fraction for the high-redshift samples is similar to $z = 0$ estimates, modulo the differences in the classification of red galaxies between the various surveys. But f_{Rcen} at $M \sim 10^{12-12.5} h^{-1} M_\odot$ must increase by nearly a factor of two, and this fraction must increase by nearly a factor of three at $M \gtrsim 10^{13} h^{-1} M_\odot$. More time elapses from $z = 0.6$ to $z = 0$ (5.8

Gyr) than elapses from $z = 1.4$ to $z = 0.6$ (3.3 Gyr). Although halo dynamical times evolve strongly with redshift, there are roughly the same number of dynamical times between SDSS and COMBO-17 as there are between COMBO-17 and the UDS (approximately 6). Thus evolution should not be ruled out as a possibility.

6.2. The Role of Satellite Galaxies in Building up the Red Sequence

At all redshifts, from $z = 2.3$ to $z = 0$, the fraction of satellites that are red is roughly consistent with $\sim 60\%$ of all satellites in the sample. This is more than double the fraction of centrals which are red, demonstrating that satellites are not simply made red before infall. Figure 13 show what fraction of the red sequence is made up satellite galaxies for each sample, as well as the fraction of those satellites that were quenched after becoming satellites. At redshifts less than $z = 2$, 60% of satellites being red translates to $\sim 30\%$ of the red sequence being made of up satellites. Roughly 70-80% of red satellites became red *after* accretion, in agreement with results for low-mass galaxies at $z = 0$ (van den Bosch et al. 2008), although the UDS results are consistent with a value as low of 10%. Thus satellite galaxies play a major role in building up the red sequence. The surprising fact is that these numbers do not vary substantially with redshift. The survival time of a subhalo scales with the dynamical time of the host halo, $(1+z)^{-1.5}$. Thus, to keep f_{Rsat} a constant requires the same redshift dependence in the quenching time, as shown in Figure 10. Given the finite lifetimes of subhalos, satellite galaxies observed at various redshifts are distinct sets of galaxies. The fraction of subhalos at $z = 0.6$ that survive to $z = 0$ is $\sim 20\%$. The fraction from $z = 0.9$ that are extant today is less than 5%. Thus the satellite galaxies analyzed in

the SDSS by van den Bosch et al. (2008) are not the same as those quantified here, yet their statistics are quite similar.

Wang et al. (2007) used clustering to constrain the quenching time at $z=0$ (cf, Figure 10). They posit that this quenching time does not evolve with redshift, and that this fixed t_Q value yields a color-density relation that largely goes away at $z \geq 1$, in qualitative agreement with the observations of Cooper et al. (2007). However, a quenching time that is fixed at 5 Gyr would be incompatible with all of the correlation functions analyzed in this paper. From Figure 9, it can be seen that *no* satellites are older than 6 Gyr at $z \gtrsim 0.6$, thus there would be no satellites quenched after infall at $z \gtrsim 0.6$. The satellite red fraction would simply trace the central red fraction, and the clustering of red galaxies would be the same as blue galaxies. The Cooper et al. (2007) measurements were made using the DEEP2 survey, thus they must be consistent with the correlation functions of Coil et al. (2008) from the same data. The lack of a strong color-density relation, as well as its gradual attenuation with increasing redshift, are compatible with the HOD results obtained here; if red central galaxies are a random sample of all central galaxies, then they produce no color-density relation. The high fraction of satellite galaxies that are red would induce a correlation between color and density, but as redshift increases the overall fraction of galaxies that are satellites decreases. Thus f_{Rsat} can remain fixed in redshift and still result in a decreasing satellite fraction within the red sequence. It should be noted, however, that the high relative bias between red and blue galaxies at $1 < z < 2$ in W09 implies that the color-density relation does exist in the UDS. Quadri et al. (2007) find the same result at higher redshift in the MUSYC survey. Further data are required to resolve this discrepancy.

The simple model for obtaining the satellite quenching time in §5.1 neglects certain effects. The quenching time may depend on both the age of a satellite and the details of its orbit (as suggested by Balogh et al. 2009), as well as the mass of the subhalo or the stellar mass of the satellite galaxy. Another explicit assumption in this model is that the quenching can only begin after a galaxy passes inside the virial radius of the parent halo. These questions will be addressed in a subsequent paper (Wetzel et al., in preparation).

6.3. Inferences from the Luminosity Function

At redshift zero, our now-standard picture is that the fraction of central galaxies that are red increases with halo mass. Above $M \approx 10^{13.5} h^{-1} M_\odot$, nearly all central galaxies are red (Zehavi et al. 2005; Weinmann et al. 2006; Yang et al. 2008). This scenario is influenced by measurements of the galaxy luminosity function; red fraction and galaxy luminosity are strongly correlated (e.g., Blanton et al. 2003b others). The results at higher redshift, however, are quite different. Above $M_B = -19.5$, the abundance of red galaxies in DEEP2 has little correlation with luminosity (Willmer et al. 2006). In Figure 1, the red fraction increases by only 9% between the faint and bright DEEP2 samples. At lower luminosities, the fraction of red galaxies does decrease. Thus, the value of $M_{\text{red}}/M_{\text{blue}}$ should increase at lower luminosity thresholds. If there is a preferential halo mass scale for star formation quenching in central galaxies, it is below the mass scale probed by the samples we have analyzed, $M \lesssim 10^{11} h^{-1} M_\odot$.

6.4. Possible Systematic Errors

A concern in this analysis is the use of diagonal error bars only, as opposed to using the full covariance matrix for each

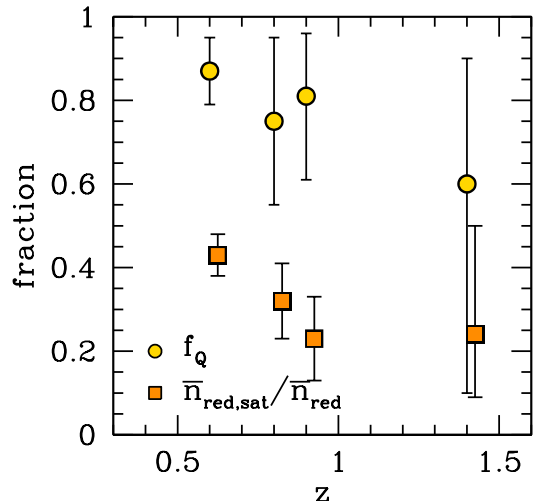


FIG. 13.— Circles indicate the fraction of red satellite galaxies that were quenched after accretion onto their parent halo, f_Q , as defined by equation (8). Squares indicate the fraction of the red sequence made up of satellite galaxies at the magnitude threshold for each sample. The redshifts for the squares are slightly offset for clarity. All errorbars are 2σ .

sample. The clustering statistics used here are known to be correlated in the two-halo term and largely uncorrelated in the one-halo term (see, eg, figures in Zehavi et al. 2005; Pheps et al. 2006; Blake et al. 2008; Tinker et al. 2009a). Thus, the use of diagonal errors over-weights the contribution of the data in the two-halo term to the χ^2 of each fit. Using our $720 h^{-1} \text{Mpc}$ simulation, we have made mock galaxy distributions that roughly match the faint DEEP2 sample. The mass resolution in this simulation is not enough to model $M \lesssim 10^{11.3} h^{-1} M_\odot$ halos, thus we are forced to modify $\langle N_{\text{cen}} \rangle_M$ of the best-fit model to obtain the proper number density of galaxies. We divide the simulation volume into $6^3 = 216$ cubic subvolumes of $120 h^{-1} \text{Mpc}$ per side. We calculate $w_p(r_p)$ within each subvolume using the Landy-Szalay estimator and accounting for the variation in the number density of galaxies in each subvolume. We are not able to obtain a robust covariance matrix for both the red and blue subsamples, thus we adopt the same (normalized) covariance matrix for both subsamples. We multiply each element by the diagonal elements measured by Coil et al. (2008), ie $C_{ij} = \hat{C}_{ij} e_i e_j$, where \hat{C}_{ij} is the normalized matrix from the mocks, $\hat{C}_{ij} = C_{ij} / \sqrt{C_{ii} C_{jj}}$. Although the covariance matrices of the red and blue subsamples should vary in detail, our test replicates the general consequences of a covariance matrix: some correlation of data in the one-halo term, with an increasing amplitude of off-diagonal terms in the two-halo term. We find virtually no difference in the $M_{\text{red}}/M_{\text{blue}}-f_{\text{Rsat}}$ constraints when using these test matrices. We conclude that our exact answers may vary slightly with use of proper estimates of C_{ij} , but the results will not change enough to alter our conclusions.

Selection effects are also a concern. If f_{Rcen} did depend on halo mass, either through a critical mass scale or a weaker dependence from a merger-like scenario, dust contamination would tend to mask this mass dependence. If galaxies are misclassified as red or quenched due to dust contamination, the large-scale amplitude of red galaxy clustering is attenuated. In terms of the HOD models presented here, and under the

assumption that f_{Rcen} was actually monotonically increasing with halo mass, dust would take low-mass blue central galaxies and place them in the red sample, reducing $M_{\text{red}}/M_{\text{blue}}$. However, this effect seems unlikely to produce f_{Rcen} in the best-fit DEEP2 model. First, if f_{Rcen} had a strong mass dependence to it, such that the fraction of red central galaxies at $M \gtrsim 10^{13} h^{-1} M_{\odot}$ were $\gtrsim 75\%$ (a value taken from the analysis of $z = 0$ clustering in the SDSS by Zehavi et al. 2005), then a mass-independent dust contamination would smooth our f_{Rcen} but not be able to remove this trend completely. More importantly, the low values of f_{Rcen} at high halo masses in the DEEP2 models ($\sim 0.15 - 0.25$) are at odds with this scenario.

One degree of freedom we have not introduced into the HOD model used here is a mass-dependence on the fraction of satellites that are red. We have performed tests with the faint DEEP2 data, introducing a mass scale below which f_{Rsat} is attenuated with a Gaussian cutoff. The constraints on this cutoff mass are weak and do not change either t_{Q} or $M_{\text{red}}/M_{\text{blue}}$. The color-dependent HOD in Zehavi et al. (2005) contained a mass-dependent parameterization in f_{Rsat} , but in most clustering samples f_{Rsat} was found to be constant. If red satellite galaxies prefer higher mass halos, the red correlation function would contain a more pronounced break between the 1-halo and 2-halo terms, and the shape of the red correlation function at small scales would not be a power-law. In the DEEP2 data, $w_p(r_p)$ for the red galaxies is a power law down to $r_p \sim 50 h^{-1} \text{kpc}$, and it does not contain a strong break at $r_p \sim 1 h^{-1} \text{Mpc}$.

Although $\alpha_{\text{sat}} = 1$ is a well-motivated prior for luminosity thresholds, assuming this power-law index for color subsamples is less cut and dry. A better fit to the faint DEEP2 data is obtained if I parameterize $\langle N_{\text{sat}} \rangle_M$ for blue and red subsamples as independent power-law functions, with different values of M_{sat} and α_{sat} for each. The χ^2 for this model is 38.6, a significant improvement on the fit from the fiducial model. However, to produce this χ^2 , both α_{sat} for the red and blue galaxies is well below unity. If $\alpha_{\text{sat}} = 1$ for the full sample, then a value of $\alpha_{\text{sat}} < 1$ for blue galaxies requires $\alpha_{\text{sat}} > 1$ for the red subsample (or vice versa). Models that produce a better fit than the fiducial model have both values below unity, with the best-fit model yielding $\alpha_{\text{sat}} = 0.39$ for the red subsample and $\alpha_{\text{sat}} = 0.48$ for the blue subsample. These values are firmly excluded from theoretical expectations and observational data (cf. §3.1). Within the range $0.9 \leq \alpha_{\text{sat}} \leq 1.1$, our constraints in Figure 7 are unchanged.

6.5. Comparison to Results from the NDWFS

Brown et al. (2008) perform HOD analysis on the clustering of red galaxies from $z = 0.2 - 1.0$ in the NDWFS imaging survey (Jannuzi & Dey 1999). At ~ 7 square degrees, this sample is much larger than all the samples analyzed in this paper. Additionally, Brown et al. (2008) use the full covariance for all halo occupation analysis. They find that the $f_{\text{Rcen}} = 0.5$ at $10^{11.9} h^{-1} M_{\odot}$, increasing with halo mass. However, the HOD model for central galaxies used in their analysis is identical to Equation (1) here. Essentially, they model red galaxy samples with an HOD constructed for a full galaxy sample. This means that f_{Rcen} must increase with mass and it will approach unity at high halo masses by construction. Without a corresponding sample of blue galaxies, it is difficult to constrain the asymptotic fraction of red central galaxies. Because Brown et al. (2008) only have photometric redshifts

of the galaxies in their sample, they can only measure $w(\theta)$, which has larger fractional errors at large scales relative to measurements of $w_p(r_p)$ over similar volumes. All HOD fits to their data are somewhat high in the two-halo term, which could be caused by the assumption that f_{Rcen} increases to unity (cf. Figure 11). However, the errors on $w(\theta)$ are large enough such that they are all statistically good fits. Corresponding measurements of the clustering of blue galaxies in the same field would help resolve the discrepancy between the results of Brown et al. (2008) and those in this paper.

7. SUMMARY

In this paper we have analyzed clustering measurements of red and blue galaxies at four different redshifts, $z = 1.4$, $z = 0.9$, $z = 0.8$, and $z = 0.6$. We have used the halo occupation distribution to determine the fraction galaxies are that red, broken into contributions of red central galaxies and red satellite galaxies. In all the samples analyzed, the higher clustering amplitude of red galaxies can be fully accounted for the the high fraction of satellite galaxies that are red; on average, the overall red fraction of each sample is $\sim 25\%$, while the fraction of satellites that are red is $\sim 60\%$. Thus the fraction of the red sequence that is satellite galaxies is $\sim 30\%$. The high value of f_{Rsat} produces enhanced clustering at both large and small scales relative to blue galaxies above the same magnitude threshold. Imparting a halo mass dependence on the fraction of central galaxies that are red enhances the relative bias between red and blue subsamples at large scales. The data are not compatible with such a scenario, favoring $M_{\text{red}}/M_{\text{blue}} = 1$ for central galaxies.

From galaxy-halo mass-to-light ratios (and stellar mass to halo mass ratios), it is inferred that galaxy formation efficiency is maximal at $M \sim 10^{12} h^{-1} M_{\odot}$ (Yang et al. 2003; van den Bosch et al. 2007; Tinker et al. 2005; Conroy & Wechsler 2009; Moster et al. 2009). This mass scale increases slowly with redshift out to $z \sim 1$ (Conroy & Wechsler 2009; Moster et al. 2009). This implies that a central galaxy's integrated star formation history is dependent on halo mass. This leads to a correlation between instantaneous star formation rate and halo mass (see Figure 8 in Conroy & Wechsler 2009). In contrast, our results imply that the fraction of galaxies that are quenched is independent of halo mass at $z \gtrsim 0.6$.

Models in which central galaxies become red at a critical halo mass scale of $\sim 10^{12} h^{-1} M_{\odot}$ are strongly excluded by the data available at $z \lesssim 1$. A scenario in which mergers produce red galaxies has a weaker dependence of red central fraction on halo mass, but these models also produce values of $M_{\text{red}}/M_{\text{blue}}$ larger than unity, values that outside the $2\text{-}\sigma$ constraints from DEEP2 and COMBO-17.

The constant value of f_{Rsat} implies that the quenching timescale for satellite galaxies depends on redshift in the same manner as the dynamical timescale of dark matter halos. Given the errors, t_{Q} for all four samples is consistent with $t_{\text{Q}} = 1.8 \text{ Gyr}$. Current estimates of t_{Q} at $z = 0$ are much longer, $\sim 5 \text{ Gyr}$, while preliminary estimates of t_{Q} at $z > 2$ are less than a Gyr.

Given the small volume of each sample, more data are required to ameliorate the possibility that sample variance is significantly influencing our results. Additionally, clustering measurements at redshift between 0 and 0.6 can shed light on discrepancies seen between $z = 0$ and the samples analyzed here. Upcoming results from the Galaxy and Mass Assembly survey (GAMA; Driver et al. 2009), as well as the clustering

of blue galaxies from the NDWFS, should show intermediate stages of evolution in both the quenching mechanism for

central galaxies and the quenching timescale for satellites.

REFERENCES

- Abadi, M. G., Moore, B., & Bower, R. G. 1999, *MNRAS*, 308, 947
- Balogh, M. L., McGee, S. L., Wilman, D., Bower, R. G., Hau, G., Morris, S. L., Mulchaey, J. S., Oemler, Jr., A., Parker, L., & Gwyn, S. 2009, *ArXiv e-prints*
- Bell, E. F., Wolf, C., Meisenheimer, K., Rix, H.-W., Borch, A., Dye, S., Kleinheinrich, M., Wisotzki, L., & McIntosh, D. H. 2004, *ApJ*, 608, 752
- Berlind, A. A. & Weinberg, D. H. 2002, *ApJ*, 575, 587
- Berlind, A. A., Weinberg, D. H., Benson, A. J., Baugh, C. M., Cole, S., Davé, R., Frenk, C. S., Jenkins, A., Katz, N., & Lacey, C. G. 2003, *ApJ*, 593, 1
- Birnboim, Y. & Dekel, A. 2003, *MNRAS*, 345, 349
- Blake, C., Collister, A., & Lahav, O. 2008, *MNRAS*, 385, 1257
- Blanton, M. R., Hogg, D. W., Bahcall, N. A., Baldry, I. K., Brinkmann, J., Csabai, I., Eisenstein, D., Fukugita, M., Gunn, J. E., Ivezić, Z., Lamb, D. Q., Lupton, R. H., Loveday, J., Munn, J. A., Nichol, R. C., Okamura, S., Schlegel, D. J., Shimasaku, K., Strauss, M. A., Vogeley, M. S., & Weinberg, D. H. 2003a, *ApJ*, 594, 186
- Blanton, M. R., Hogg, D. W., Bahcall, N. A., Brinkmann, J., Britton, M., Connolly, A. J., Csabai, I., Fukugita, M., Loveday, J., Meiksin, A., Munn, J. A., Nichol, R. C., Okamura, S., Quinn, T., Schneider, D. P., Shimasaku, K., Strauss, M. A., Tegmark, M., Vogeley, M. S., & Weinberg, D. H. 2003b, *ApJ*, 592, 819
- Bower, R. G., Benson, A. J., Malbon, R., Helly, J. C., Frenk, C. S., Baugh, C. M., Cole, S., & Lacey, C. G. 2006, *MNRAS*, 370, 645
- Brown, M. J. I., Zheng, Z., White, M., Dey, A., Jannuzi, B. T., Benson, A. J., Brand, K., Brodwin, M., & Croton, D. J. 2008, *ApJ*, 682, 937
- Butcher, H. & Oemler, Jr., A. 1978, *ApJ*, 226, 559
- , 1984, *ApJ*, 285, 426
- Cattaneo, A., Dekel, A., Devriendt, J., Guiderdoni, B., & Blaizot, J. 2006, *MNRAS*, 370, 1651
- Cohn, J. D., Bagla, J. S., & White, M. 2001, *MNRAS*, 325, 1053
- Coil, A. L., Newman, J. A., Croton, D., Cooper, M. C., Davis, M., Faber, S. M., Gerke, B. F., Koo, D. C., Padmanabhan, N., Wechsler, R. H., & Weiner, B. J. 2008, *ApJ*, 672, 153
- Collister, A. A. & Lahav, O. 2005, *MNRAS*, 361, 415
- Conroy, C. & Wechsler, R. H. 2009, *ApJ*, 696, 620
- Conroy, C., Wechsler, R. H., & Kravtsov, A. V. 2006, *ApJ*, 647, 201
- Cooper, M. C., Newman, J. A., Coil, A. L., Croton, D. J., Gerke, B. F., Yan, R., Davis, M., Faber, S. M., Guhathakurta, P., Koo, D. C., Weiner, B. J., & Willmer, C. N. A. 2007, *MNRAS*, 376, 1445
- Cooper, M. C., Newman, J. A., Croton, D. J., Weiner, B. J., Willmer, C. N. A., Gerke, B. F., Madgwick, D. S., Faber, S. M., Davis, M., Coil, A. L., Finkbeiner, D. P., Guhathakurta, P., & Koo, D. C. 2006, *MNRAS*, 370, 198
- Cooray, A. & Sheth, R. 2002, *Phys. Rep.*, 372, 1
- Croton, D. J., Springel, V., White, S. D. M., De Lucia, G., Frenk, C. S., Gao, L., Jenkins, A., Kauffmann, G., Navarro, J. F., & Yoshida, N. 2006, *MNRAS*, 365, 11
- Davis, M. & Peebles, P. J. E. 1983, *ApJ*, 267, 465
- De Lucia, G. & Blaizot, J. 2007, *MNRAS*, 375, 2
- De Lucia, G., Kauffmann, G., Springel, V., White, S. D. M., Lanzoni, B., Stoehr, F., Tormen, G., & Yoshida, N. 2004, *MNRAS*, 348, 333
- Dekel, A. & Birnboim, Y. 2006, *MNRAS*, 368, 2
- , 2008, *MNRAS*, 383, 119
- Dekel, A., Birnboim, Y., Engel, G., Freundlich, J., Goerdt, T., Mumcuoglu, M., Neistein, E., Pichon, C., Teyssier, R., & Zinger, E. 2008, *Nature*, accepted (arXiv:0808.0553)
- Driver, S. P., the GAMA Team, Baldry, I. K., Bamford, S., Bland-Hawthorn, J., Bridges, T., Cameron, E., Conselice, C., Couch, W. J., Croom, S., Cross, N. J. G., Driver, S. P., Dunne, L., Eales, S., Edmondson, E., Ellis, S. C., Frenk, C. S., Graham, A. W., Jones, H., Hill, D., Hopkins, A., van Kampen, E., Kuijken, K., Lahav, O., Liske, J., Loveday, J., Nichol, B., Norberg, P., Oliver, S., Parkinson, H., Peacock, J. A., Phillipps, S., Popescu, C. C., Prescott, M., Proctor, R., Sharp, R., Staveley-Smith, L., Sutherland, W., Tuffs, R. J., & Warren, S. 2009, in *IAU Symposium*, Vol. 254, IAU Symposium, ed. J. Andersen, J. Bland-Hawthorn, & B. Nordström, 469–474
- Dunkley, J., Komatsu, E., Nolte, M. R., Spergel, D. N., Larson, D., Hinshaw, G., Page, L., Bennett, C. L., Gold, B., Jarosik, N., Weiland, J. L., Halpern, M., Hill, R. S., Kogut, A., Limon, M., Meyer, S. S., Tucker, G. S., Wollack, E., & Wright, E. L. 2008, *ApJS*, in press
- Eke, V. R., Baugh, C. M., Cole, S., Frenk, C. S., Norberg, P., Peacock, J. A., Baldry, I. K., Bland-Hawthorn, J., Bridges, T., Cannon, R., Colless, M., Collins, C., Couch, W., Dalton, G., de Propris, R., Driver, S. P., Efstathiou, G., Ellis, R. S., Glazebrook, K., Jackson, C., Lahav, O., Lewis, I., Lumsden, S., Maddox, S., Madgwick, D., Peterson, B. A., Sutherland, W., & Taylor, K. 2004, *MNRAS*, 348, 866
- Fakhouri, O. & Ma, C.-P. 2007, *MNRAS*, submitted (ArXiv:0710.4567)
- Fisher, K. B. 1995, *ApJ*, 448, 494
- Gao, L., White, S. D. M., Jenkins, A., Stoehr, F., & Springel, V. 2004, *MNRAS*, 355, 819
- Gerke, B. F., Newman, J. A., Faber, S. M., Cooper, M. C., Croton, D. J., Davis, M., Willmer, C. N. A., Yan, R., Coil, A. L., Guhathakurta, P., Koo, D. C., & Weiner, B. J. 2007, *MNRAS*, 376, 1425
- Gunn, J. E. & Gott, J. R. I. 1972, *ApJ*, 176, 1
- Hamilton, A. J. S. 1998, in *Astrophysics and Space Science Library*, Vol. 231, *The Evolving Universe*, ed. D. Hamilton, 185–+
- Hansen, S. M., Sheldon, E. S., Wechsler, R. H., & Koester, B. P. 2009, *ApJ*, 699, 1333
- Harker, G., Cole, S., & Jenkins, A. 2007, *MNRAS*, 382, 1503
- Hawkins, E., Maddox, S., Cole, S., Lahav, O., Madgwick, D. S., Norberg, P., Peacock, J. A., Baldry, I. K., Baugh, C. M., Bland-Hawthorn, J., Bridges, T., Cannon, R., Colless, M., Collins, C., Couch, W., Dalton, G., De Propris, R., Driver, S. P., Efstathiou, G., Ellis, R. S., Frenk, C. S., Glazebrook, K., Jackson, C., Jones, B., Lewis, I., Lumsden, S., Percival, W., Peterson, B. A., Sutherland, W., & Taylor, K. 2003, *MNRAS*, 346, 78
- Hopkins, P. F., Cox, T. J., Kereš, D., & Hernquist, L. 2008a, *ApJS*, 175, 390
- Hopkins, P. F., Hernquist, L., Cox, T. J., & Kereš, D. 2008b, *ApJS*, 175, 356
- Jannuzi, B. T. & Dey, A. 1999, in *Astronomical Society of the Pacific Conference Series*, Vol. 191, *Photometric Redshifts and the Detection of High Redshift Galaxies*, ed. R. Weymann, L. Storrie-Lombardi, M. Sawicki, & R. Brunner, 111–+
- Kaiser, N. 1987, *MNRAS*, 227, 1
- Kauffmann, G., Heckman, T. M., White, S. D. M., Charlot, S., Tremonti, C., Brinchmann, J., Bruzual, G., Peng, E. W., Seibert, M., Bernardi, M., Blanton, M., Brinkmann, J., Castander, F., Csabai, I., Fukugita, M., Ivezić, Z., Munn, J. A., Nichol, R. C., Padmanabhan, N., Thakar, A. R., Weinberg, D. H., & York, D. 2003a, *MNRAS*, 341, 33
- Kauffmann, G., Heckman, T. M., White, S. D. M., Charlot, S., Tremonti, C., Peng, E. W., Seibert, M., Brinkmann, J., Nichol, R. C., SubbaRao, M., & York, D. 2003b, *MNRAS*, 341, 54
- Kereš, D., Katz, N., Fardal, M., Dave, R., & Weinberg, D. H. 2008, *MNRAS*, submitted (arXiv:0809.1430)
- Kereš, D., Katz, N., Weinberg, D. H., & Davé, R. 2005, *MNRAS*, 363, 2
- Kimm, T., Somerville, R. S., Yi, S. K., van den Bosch, F. C., Salim, S., Fontanot, F., Monaco, P., Mo, H., Pasquali, A., Rich, R. M., & Yang, X. 2009, *MNRAS*, 394, 1131
- Kochanek, C. S., White, M., Huchra, J., Macri, L., Jarrett, T. H., Schneider, S. E., & Mader, J. 2003, *ApJ*, 585, 161
- Koester, B. P., McKay, T. A., Annis, J., Wechsler, R. H., Evrard, A., Bleem, L., Becker, M., Johnston, D., Sheldon, E., Nichol, R., Miller, C., Scranton, R., Bahcall, N., Barentine, J., Brewington, H., Brinkmann, J., Harvanek, M., Kleinman, S., Krzesinski, J., Long, D., Nitta, A., Schneider, D. P., Sneddin, S., Voges, W., & York, D. 2007, *ApJ*, 660, 239
- Kravtsov, A. V., Berlind, A. A., Wechsler, R. H., Klypin, A. A., Gottlöber, S., Algood, B., & Primack, J. R. 2004, *ApJ*, 609, 35
- Kriek, M., van der Wel, A., van Dokkum, P. G., Franx, M., & Illingworth, G. D. 2008, *ApJ*, 682, 896
- Kriek, M., van Dokkum, P. G., Franx, M., Quadri, R., Gawiser, E., Herrera, D., Illingworth, G. D., Labbé, I., Lira, P., Marchesini, D., Rix, H.-W., Rudnick, G., Taylor, E. N., Toft, S., Urry, C. M., & Wuyts, S. 2006, *ApJ*, 649, L71
- Labbé, I., Huang, J., Franx, M., Rudnick, G., Barmby, P., Daddi, E., van Dokkum, P. G., Fazio, G. G., Schreiber, N. M. F., Moorwood, A. F. M., Rix, H.-W., Röttgering, H., Trujillo, I., & van der Werf, P. 2005, *ApJ*, 624, L81
- Landy, S. D. & Szalay, A. S. 1993, *ApJ*, 412, 64
- Li, C., Kauffmann, G., Jing, Y. P., White, S. D. M., Börner, G., & Cheng, F. Z. 2006, *MNRAS*, 368, 21
- Lin, Y.-T., Mohr, J. J., & Stanford, S. A. 2004, *ApJ*, 610, 745
- Madgwick, D. S., Somerville, R., Lahav, O., & Ellis, R. 2003, *MNRAS*, 343, 871
- Magliocchetti, M. & Porciani, C. 2003, *MNRAS*, 346, 186
- Maller, A. H. 2008, in *Astronomical Society of the Pacific Conference Series*, Vol. 396, *Astronomical Society of the Pacific Conference Series*, ed. J. G. Funes & E. M. Corsini, 251–+
- Maller, A. H., Berlind, A. A., Blanton, M. R., & Hogg, D. W. 2009, *ApJ*, 691, 394
- Marchesini, D., van Dokkum, P., Quadri, R., Rudnick, G., Franx, M., Lira, P., Wuyts, S., Gawiser, E., Christlein, D., & Toft, S. 2007, *ApJ*, 656, 42
- Marín, F. A., Wechsler, R. H., Frieman, J. A., & Nichol, R. C. 2008, *ApJ*, 672, 849
- Mihos, J. & Hernquist, L. 1996, *ApJ*, 464, 641
- More, S., van den Bosch, F. C., Cacciato, M., Mo, H. J., Yang, X., & Li, R. 2009, *MNRAS*, 392, 801
- Moster, B. P., Somerville, R. S., Maulbetsch, C., van den Bosch, F. C., Maccio, A. V., Naab, T., & Oser, L. 2009, *ApJ*, submitted, ArXiv:0903.4682
- Nagai, D. & Kravtsov, A. V. 2005, *ApJ*, 618, 557
- Negroponante, J. & White, S. D. M. 1983, *MNRAS*, 205, 1009
- Noeske, K. G., Faber, S. M., Weiner, B. J., Koo, D. C., Primack, J. R., Dekel, A., Papovich, C., Conselice, C. J., Le Floch, E., Rieke, G. H., Coil, A. L., Lotz, J. M., Somerville, R. S., & Bundy, K. 2007, *ApJ*, 660, L47

- Norberg, P., Baugh, C. M., Hawkins, E., Maddox, S., Madgwick, D., Lahav, O., Cole, S., Frenk, C. S., Baldry, I., Bland-Hawthorn, J., Bridges, T., Cannon, R., Colless, M., Collins, C., Couch, W., Dalton, G., De Propris, R., Driver, S. P., Efstathiou, G., Ellis, R. S., Glazebrook, K., Jackson, C., Lewis, I., Lumsden, S., Peacock, J. A., Peterson, B. A., Sutherland, W., & Taylor, K. 2002, *MNRAS*, 332, 827
- Papovich, C., Moustakas, L. A., Dickinson, M., Le Floe'h, E., Rieke, G. H., Daddi, E., Alexander, D. M., Bauer, F., Brandt, W. N., Dahlen, T., Egami, E., Eisenhardt, P., Elbaz, D., Ferguson, H. C., Giavalisco, M., Lucas, R. A., Mobasher, B., Pérez-González, P. G., Stutz, A., Rieke, M. J., & Yan, H. 2006, *ApJ*, 640, 92
- Peacock, J. A. & Smith, R. E. 2000, *MNRAS*, 318, 1144
- Pheps, S., Peacock, J. A., Meisenheimer, K., & Wolf, C. 2006, *A&A*, 457, 145
- Quadri, R., van Dokkum, P., Gawiser, E., Franx, M., Marchesini, D., Lira, P., Rudnick, G., Herrera, D., Maza, J., Kriek, M., Labbé, I., & Francke, H. 2007, *ApJ*, 654, 138
- Quadri, R. F., Williams, R. J., Lee, K.-S., Franx, M., van Dokkum, P., & Brammer, G. B. 2008, *ApJ*, 685, L1
- Scoccimarro, R. 2004, *Phys. Rev. D*, 70, 083007
- Scoccimarro, R., Sheth, R. K., Hui, L., & Jain, B. 2001, *ApJ*, 546, 20
- Scranton, R. 2003, *MNRAS*, 339, 410
- Seljak, U. 2000, *MNRAS*, 318, 203
- Seljak, U., Hamaus, N., & Desjacques, V. 2009, *ArXiv e-prints*
- Skibba, R. A. & Sheth, R. K. 2009, *MNRAS*, 392, 1080
- Somerville, R. S., Hopkins, P. F., Cox, T. J., Robertson, B. E., & Hernquist, L. 2008, *MNRAS*, 1241
- Springel, V. 2000, *MNRAS*, 312, 859
- Strateva, I., Ivezić, Ž., Knapp, G. R., Narayanan, V. K., Strauss, M. A., Gunn, J. E., Lupton, R. H., Schlegel, D., Bahcall, N. A., Brinkmann, J., Brunner, R. J., Budavári, T., Csabai, I., Castander, F. J., Doi, M., Fukugita, M., Györy, Z., Hamabe, M., Hennessy, G., Ichikawa, T., Kunszt, P. Z., Lamb, D. Q., McKay, T. A., Okamura, S., Racusin, J., Sekiguchi, M., Schneider, D. P., Shimasaku, K., & York, D. 2001, *AJ*, 122, 1861
- Tinker, J., Kravtsov, A. V., Klypin, A., Abazajian, K., Warren, M., Yepes, G., Gottlöber, S., & Holz, D. E. 2008a, *ApJ*, 688, 709
- Tinker, J. L., Conroy, C., Norberg, P., Patiri, S. G., Weinberg, D. H., & Warren, M. S. 2008b, *ApJ*, 686, 53
- Tinker, J. L., Norberg, P., Weinberg, D. H., & Warren, M. S. 2007, *ApJ*, 659, 877
- Tinker, J. L., Wechsler, R. H., & Zheng, Z. 2009a, *ApJ*, (submitted), arXiv:0902.1748
- Tinker, J. L., Weinberg, D. H., & Warren, M. S. 2006, *ApJ*, 647, 737
- Tinker, J. L., Weinberg, D. H., Zheng, Z., & Zehavi, I. 2005, *ApJ*, 631, 41
- Tinker, J. T. et al. 2009b, in preparation
- Toomre, A. & Toomre, J. 1972, *ApJ*, 178, 623
- Vale, A. & Ostriker, J. P. 2006, *MNRAS*, 371, 1173
- van den Bosch, F. C., Aquino, D., Yang, X., Mo, H. J., Pasquali, A., McIntosh, D. H., Weinmann, S. M., & Kang, X. 2008, *MNRAS*, 387, 79
- van den Bosch, F. C., Yang, X., Mo, H. J., Weinmann, S. M., Macciò, A. V., More, S., Cacciato, M., Skibba, R., & Kang, X. 2007, *MNRAS*, 376, 841
- Wang, L., Li, C., Kauffmann, G., & De Lucia, G. 2006, *MNRAS*, 371, 537
- 2007, *MNRAS*, 377, 1419
- Weinmann, S. M., van den Bosch, F. C., Yang, X., & Mo, H. J. 2006, *MNRAS*, 366, 2
- Wetzel, A. & White, M. 2009, *MNRAS*, submitted, ArXiv:0907.0702
- Wetzel, A. R., Cohn, J. D., & White, M. 2009, *MNRAS*, 395, 1376
- White, M. 2002, *ApJS*, 143, 241
- White, M., Hernquist, L., & Springel, V. 2001, *ApJ*, 550, L129
- Williams, R. J., Quadri, R. F., Franx, M., van Dokkum, P., & Labbé, I. 2009, *ApJ*, 691, 1879
- Willmer, C. N. A., Faber, S. M., Koo, D. C., Weiner, B. J., Newman, J. A., Coil, A. L., Connolly, A. J., Conroy, C., Cooper, M. C., Davis, M., Finkbeiner, D. P., Gerke, B. F., Guhathakurta, P., Harker, J., Kaiser, N., Kassir, S., Konidaris, N. P., Lin, L., Luppino, G., Madgwick, D. S., Noeske, K. G., Phillips, A. C., & Yan, R. 2006, *ApJ*, 647, 853
- Wolf, C., Meisenheimer, K., Kleinheinrich, M., Borch, A., Dye, S., Gray, M., Wisotzki, L., Bell, E. F., Rix, H.-W., Cimatti, A., Hasinger, G., & Szokoly, G. 2004, *A&A*, 421, 913
- Wolf, C., Meisenheimer, K., Rix, H.-W., Borch, A., Dye, S., & Kleinheinrich, M. 2003, *A&A*, 401, 73
- Yang, X., Mo, H. J., & van den Bosch, F. C. 2003, *MNRAS*, 339, 1057
- 2008, *ApJ*, 676, 248
- Zehavi, I., Zheng, Z., Weinberg, D. H., Frieman, J. A., Berlind, A. A., Blanton, M. R., Scoccimarro, R., Sheth, R. K., Strauss, M. A., Kayo, I., Suto, Y., Fukugita, M., Nakamura, O., Bahcall, N. A., Brinkmann, J., Gunn, J. E., Hennessy, G. S., Ivezić, Ž., Knapp, G. R., Loveday, J., Meiksin, A., Schlegel, D. J., Schneider, D. P., Szapudi, I., Tegmark, M., Vogeley, M. S., & York, D. G. 2005, *ApJ*, 630, 1
- Zhao, D. H., Jing, Y. P., Mo, H. J., & Boerner, G. 2008, *ArXiv e-prints*
- Zheng, Z. 2004, *ApJ*, 610, 61
- Zheng, Z., Berlind, A. A., Weinberg, D. H., Benson, A. J., Baugh, C. M., Cole, S., Davé, R., Frenk, C. S., Katz, N., & Lacey, C. G. 2005, *ApJ*, 633, 791
- Zheng, Z., Coil, A. L., & Zehavi, I. 2007, *ApJ*, 667, 760
- Zheng, Z., Zehavi, I., Eisenstein, D. J., Weinberg, D. H., & Jing, Y. 2008, *ApJ*, submitted, arXiv:0809.1868 [astro-ph]